

INTERNATIONAL SCIENTIFIC JOURNAL

MECHANIZATION IN AGRICULTURE

& CONSERVING OF THE RESOURCES



Issue 1
2022

Year LXVIII, ISSNprint2603-3704, ISSN web 2603-3712

SCIENTIFIC TECHNICAL UNION OF MECHANICAL ENGINEERING
BULGARIAN ASSOCIATION OF MECHANIZATION IN AGRICULTURE



PUBLISHERS

SCIENTIFIC-TECHNICAL UNION OF MECHANICAL ENGINEERING "INDUSTRY-4.0"
BUGLARINA ASSOCIATION OF AGRICULTURAL MACHINERY

ISSN (PRINT) 2603-3704, ISSN (ONLINE) 2603-3712

YEAR LXVIII ISSUE 1 / 2022

EDITORIAL BOARD

Chief Editor: Prof. Dr. eng Miho Mihov

Responsible secretary: Corresp. Memb. Prof. D.Sc. Hristo Beloev

MEMBERS:

Acad. D.Sc. Jemal Katsitadze – Georgia
Acad. D.Sc. Sayakhat Nukeshev - Kazakhstan
Acad. D.Sc. Volodymyr Bulgakov – Ukraine
Acad. D.Sc. Valeriy Adamchuk – Ukraine
Prof. Abdullah Sessiz - Turkey
Prof. Abdulrahman Al-soqeer - Saudi Arabia
Prof. Alexander Tokarev - Russia
Prof. Alexey Vassilev - Russia
Assoc.Prof. Angel Trifonov - Bulgaria
Prof. Anupam Kumar Nema - India
Prof. Ayrat Valiev - Russia
Prof. Barbro Ulén - Sweden
Prof. Carmen Puia - Romania
Prof. Cheslav Vashkievich - Poland
Prof. Cumhuri Aydinalp - Turkey
Prof. Daisuke Higaki - Japan
Prof. Davor Romic - Croatia
Prof. Domenico Pessina - Italy
Dr. Finn Plauborg - Denmark
Assoc.Prof. Ganka Baeva - Bulgaria
Assoc. Prof. Dr. Mariusz Szymanek - Poland
Prof. Georgi Tassev - Bulgaria
Prof. Haiyan Huang - China
Prof. Hoang Thai Dai - Vietnam

Prof. Iliya Malinov – Bulgaria
Eng. Ivan Opacak - Croatia
Prof. PhD Iurie Melnic - Moldova
Assoc.Prof. Ivan Ivanov - Bulgaria
Prof. Jan Szczepaniak - Poland
Prof. Komil Muminov - Uzbekistan
Prof. Krassimira Georgieva - Bulgaria
Prof. Maja Manojlović - Serbia
Prof. Mihail Iliev - Bulgaria
Prof. Mohammad Salem Al-Hwaiti - Jordan
Prof. Papamichail Dimitris - Greece
Prof. Pavel Tlustos - Czech Republic
Prof. Plamen Kangalov - Bulgaria
Prof. Ralph Meissner - Germany
Prof. Rossen Ivanov - Bulgaria
Prof. Svetla Rousseva - Bulgaria
Prof. Tadeusz Pawłowski - Poland
Prof. Tamara Persikova - Belarus
Prof. Valentina Kundius - Russia
Prof. Wojciech Tanaś - Poland
Prof. Yerbol Sarkynov - Kazakhstan
Prof. Zdenko Tkach - Slovakia
Prof. Zinta Gaile - Latvia
Prof. Zivko Davchev - Macedonia

The journal "MECHANIZATION IN AGRICULTURE & CONSERVING OF THE RESOURCES" is continuer of the journals "Mechanized farming" (1948-1957), "Mechanization and electrification of agriculture" (1959-1980) and "Mechanization of agriculture" (1981-1991)

108, Rakovski Str., 1000 Sofia, Bulgaria
tel. (+359 2) 987 72 90, tel./fax (+359 2) 986 22 40,

office@stumejournals.com
WWW.STUMEJOURNALS.COM

CONTENTS

MECHANIZATION IN AGRICULTURE

Mathematical modeling of features of electrophysical processes in a vibration plow with piezoelectric actuator Vladimir Galchenko, Sergei Yashchenko, Sergey Filimonov, Nadiia Filimonova	3
Research of combustion engine oil quality over exploitation period Mažeika Darius, Balnys Rytis, Kandrotaitė Janutienė Rasa	7
Kinematic analysis of the slider-crank mechanism of an internal combustion (IC) engine using modern software Marko Lučić	11
Identifying Photovoltaic Water Pumping (PVWP) Systems. Opportunities in Albanian’s Agriculture Context. Ilirian Konomi, Lorenc Malka, Ermonela Rrapaj	18
Study of the magnetic field of a magnetic treatment device for agricultural materials Nedyalko Nedyalkov, Miho Mihov, Viktoriya Kancheva	24
An overview of agriculture sector in terms of fuel type and systems used for irrigation purposes. Case study: Divjaka region, Albania Ilirian Konomi, Elena Bebi, Lorenc Malka, Ermonela Rrapaj	27
Investigation of the movement of a tomato plant during the transition between transport devices Ivan Morteve	32

CONSERVING OF THE RESOURCES

Studies to establish the evapotranspiration of strawberries grown in open areas Rumiana Kireva, Miho Mihov	35
--	----

Mathematical modeling of features of electrophysical processes in a vibration plow with piezoelectric actuator

Vladimir Galchenko, Sergei Yashchenko, Sergey Filimonov, Nadiia Filimonova
Cherkasy State Technological University,
Cherkasy, Ukraine
s.filimonov@chdtu.edu.ua

Abstract: In the process of studying multiphysical processes, including electrophysical ones, the resonance frequency at which the piezoelectric actuator maximally influences the amplitude of oscillations of the plow blade was established in the COMSOL Multiphysics software package. The maximum amplitude of oscillations of the plow-piezo actuator system and the rational location of the piezo actuator on the dump, which provides an efficient vibration process, have also been determined. The performed numerical experiments allowed to obtain approximation expressions for simplified determination of the amplitude of oscillations of the system depending on the coordinates of the piezo actuator on the heap. The research results can be used in the design of vibrating soil cultivation bodies in agricultural machinery.

Keywords: PIEZOCERAMIC ACTUATOR, VIBRATION TECHNOLOGIES, COMSOL MULTIPHYSICS, APPROXIMATE DEPENDENCES.

1. Introduction

Agriculture is one of the leading branches of the production sphere, which is engaged in the cultivation of agricultural crops. The main task of agriculture is to provide the population with food and raw materials for industry. The food security of the state and its citizens depends on the state of agriculture [1]. One of the main problems of agriculture is the complexity and efficiency of land cultivation. The process of loosening the soil with a wedge is one of the most common ways to improve its properties [2]. Loosening the soil is created through the use of conventional plows. Therefore, their improvement as the main devices for soil cultivation is a reliable way to improve the efficiency of tillage [3]. One of the areas of improvement is to combine plows with actuators and thus obtain vibrating plows, which are more efficient in processing than conventional ones.

An actuator is an actuator or its active element that converts one type of energy (electrical, magnetic, etc.) into another (most often - into mechanical), which leads to the performance of a certain action specified by the control signal. [4-8]. The properties of the actuator depend on the physical effect on which they work.

Modern vibrating plows are improved through the use of electromagnetic actuators and hydraulic actuators. One alternative type of actuator is the piezo actuator. The piezo actuator is a piezomechanical device that operates on the basis of the reverse piezoelectric effect and is designed to actuate mechanisms and systems, ie the determinants of its performance are electrophysical and mechanical processes in their interaction. The main advantages of piezoelectric actuators (PA) are the ability to create significant effort when moving, while having a minimum size. This allows them to be easily integrated into power systems [4-8]. In addition, PAs are characterized by simplicity of design and high reliability during operation.

However, the theoretical basis for the use of piezoelectric actuators in soil cultivation bodies is almost non-existent. Thus, the creation of certain theoretical recommendations based on complex mathematical modeling of electrophysical and mechanical processes in the system "plow dump-PA" for the design of vibrating plows using PA is relevant.

2. Description of the analyzed vibrating plows

Experimentally established [9], that when using vibrations in plows the friction of sliding of soil on a ploughshare and a shelf which are elements of a plow which is the main component in the general size of traction resistance considerably decreases. The stickiness of the working bodies is also reduced. This leads to a reduction in fuel consumption, reduces wear of parts of agricultural machinery and cultivation bodies, ie increases its service life and reduces the processing time of the site. In this regard, new designs of plows with vibrating working bodies have recently appeared. One such plow with an electromagnetic actuator [9] presented in fig. 1.

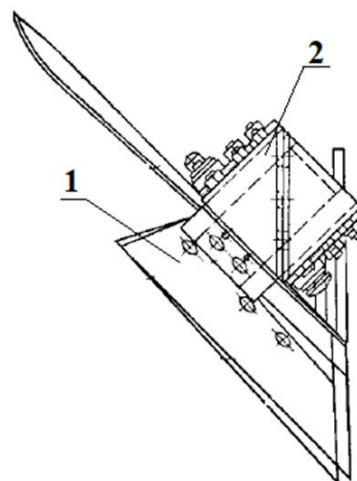


Fig.1. Vibrating plow body with electromagnetic vibrator: 1 - blade; 2 - electromagnetic actuator

The principle of operation of the vibrating plow with an electromagnetic vibrator is as follows. Current pulses are fed to the coil of the vibrator electromagnet, forcing the armature together with the moving part of the working body with a frequency of about 50 oscillations per second. In the absence of current pulses under the action of the soil reaction, the actuator armature is squeezed. The obtained oscillations of the moving part of the working body are directed normally to the blade of the ploughshare. The obtained experimental data showed a positive effect [9]. However, it should be noted that the main disadvantages of this design are quite large dimensions, relatively high current consumption and low oscillation frequency of the blade.

Also noteworthy are two general-purpose plow designs with hydraulic semi-automatic and automatic vibrator adjustment. The design of these plows is developed on the basis of plow PN-3-35. The rack of each case is cut into two parts, which are hinged to each other. The upper part of the rack is attached to the plow frame, and the lower is connected to it by a hinge, which is located below the conditional center of resistance of the body. Displacement of the hinge from the center of resistance provides the necessary force for automatic adjustment of vibration modes [9]. The design of a plow with such an actuator is quite complex and, as a result, not very reliable.

In the works [1, 10] the development of a vibrating plow with the use of PA is presented. Unlike other vibrating plows, its PA version is much smaller and heavier, has a high efficiency, is characterized by a wide range of control excitation frequencies and the creation of significant forces during vibration. However, these studies did not conduct or present the results of studies that substantiate the approximate optimal location of the PA on a regular plow heap cultivation tool based on multiphysical modeling of its characteristic processes that directly affect its efficiency. Therefore,

the implementation of the above tasks is an urgent application problem that needs to be solved.

Materials and methods. To study the influence of electrophysical and mechanical processes in their interaction on the vibrational oscillations of the system "plow dump-PA" was conducted a series of numerical experiments using the software package COMSOL Multiphysics 3.5.

The COMSOL program interface combines the functions of modeling modules of solid mechanics COMSOL's Solid Mechanics and electrostatics Electrostatics into one computing tool for modeling piezoelectric materials. Modeling of piezoelectric devices in COMSOL Multiphysics 3.5 is carried out using the Piezoelectric Effects module. Since the operation of the PA is based on the inverse piezoelectric effect, so in the module Piezoelectric Effects selected mode Stress-Charge Form [11, 12]. The piezoelectric element is characterized by the connection between mechanical deformations and the electric field, which is determined by the material and constitutive relations [13-15]:

$$\begin{aligned}
 \nabla \cdot D &= \rho; \\
 \nabla \cdot T &= 0; \\
 T &= c_E S - e^T E; \\
 D &= e S - \epsilon_S E; \\
 c_E &= S_E^{-1}; \\
 e &= d S_E^{-1}; \\
 \epsilon_S &= \epsilon_T - d S_E^{-1} d^T;
 \end{aligned}
 \tag{1}$$

where T – mechanical stress;

S – deformation;

E – electric field strength;

D – electric field displacement;

c_E – elastic matrix (tensor of the 4th rank c_{ijkl});

e – communication matrix (tensor of 3rd rank e_{ijk});

d – matrix of piezo modules (tensor of 3rd rank d_{imn});

ϵ_S – dielectric constant matrix (tensor of the 2nd rank ϵ_{ij});

ρ – free charge density;

ϵ_T - dielectric constant of piezoelectric material.

For multiphysical finite element mathematical modeling of processes, as in [12], Lagrange finite elements with elementary basic functions of the second order - Lagrange-Quadratic - were used. The calculated mesh of finite elements in the item "Mesh" was chosen orthogonalized with the normal size of the elements Normal. Direct was used as the Solver, in which the numerical SPOOLES method was chosen to solve a system of linear equations with sparse matrices.

Modeling of the piezoceramic plate was performed under the condition of its production from PZT-5H brand material. Structural Steel material was used for the metal part of the investigated system, ie the plow blade, for similar purposes. The overall dimensions and geometry of this cultivation organ are illustrated in fig. 2, which also indicates one of the options for placement of PA.

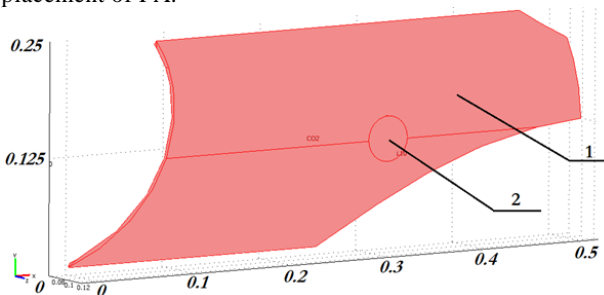


Fig. 2. Plow blade with piezoelectric actuator:
1 - dump; 2 - disk piezoelectric actuator

The studied three-dimensional model of the system "plow dump-PA" is represented by a set of finite elements obtained by constructing a grid with tetragonal partition. The corresponding CAD model of the system is illustrated in Fig. 3.

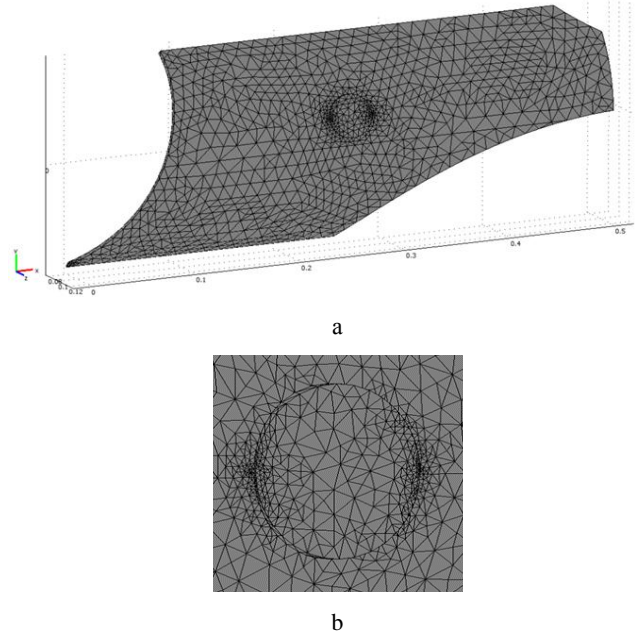


Fig. 3. Three-dimensional CAD-model of the system "plow dump-PA": a - general view; b - area of PA placement

The following limit conditions were set during modeling: for electrical processes - supply of electric voltage and zero potential to diametrically opposite sides of the PA, respectively electric potential and ground (the side of the PA adjacent to the surface of the dump); for mechanical processes, the lower surface of the piezoceramic disk, which is the support and placed on the shaft, was fixed, and the opposite - the possibility of free movement.

Results. To conduct modeling, we first determine the overall dimensions of the PA. Among the standard sizes of piezoceramic disks produced by the industry, we will choose the one that has the maximum diameter and allows at the same time a full-fledged fit to the curved surface of the blade at any point of its connection. These conditions are satisfied by PA with a diameter of 45 mm. Conditionally apply a uniform grid on the surface of the dump with the dimensions of the cell 45x45 mm, which allows you to inscribe in it a circle with a diameter equal to the diameter of the selected piezo-frame disk. This grid, shown in fig. 4, determines the possible locations of the PA on the dump when searching for its position, which provides the maximum vibration effect of the entire system "plow dump-PA".

Grid cells with code A2, A11, B2, C2, C10, C11, D2, D8-D9, E1, E7, F1-F6 cannot be considered as possible for PA placement for obvious reasons. In other cells of the grid, except for those that do not overlap on the surface of the dump, alternately placed PA, followed by computer simulation of multiphysical processes, which are crucial for the implementation of the necessary oscillations of the system under study.

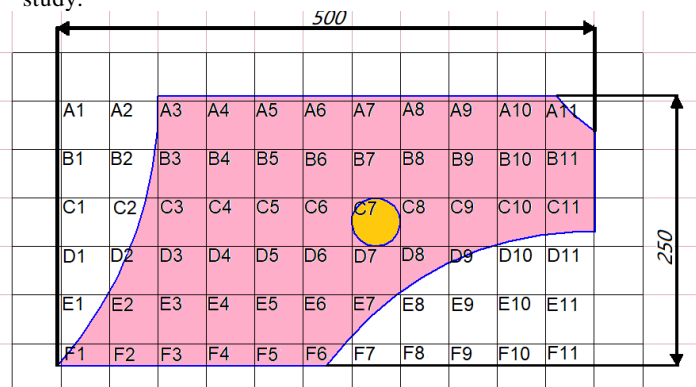


Fig. 4. Drawing a grid and coding its cells on a plow dump

At the first stage of modeling to determine the limits of the operating frequency range of the system numerical experiments were performed in Eigenfrequency mode, ie determining the natural frequencies that depend only on material properties, geometry and dimensions of PA, mechanical boundary conditions. This makes it possible to carefully study the amplitude-frequency characteristics of the system "plow blade-PA" near the natural frequencies, where it is possible to observe resonance. The values of the first six natural frequencies of the system were determined. For example, for cell C6, they are in the range from 100 Hz to 1000 Hz.

Further in the mode of Frequency Response Analysis, ie analysis of the frequency response when applying to the PA alternating sinusoidal voltage, the next stage of research was conducted to determine such a cell grid to accommodate the PA, which is best to achieve maximum propagation of oscillations.

Some examples of the results of numerical experiments are shown in fig. 5.

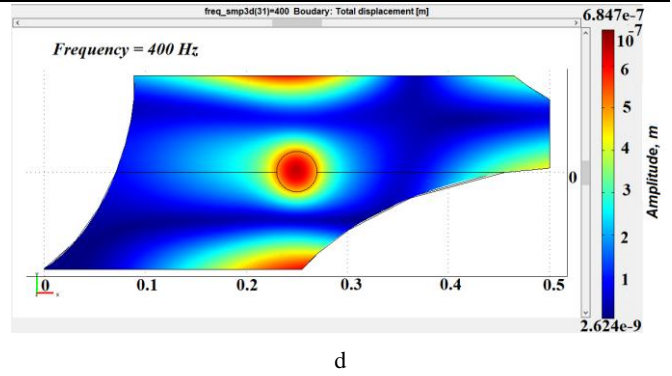


Fig. 5. Examples of determining the oscillations of the system "plow dump-PA", which were obtained in different cells of the grid: a - cell C3; b - cell C4; c - cell C5; d - cell C6

The image of Fig. 5 contain the given color scale of gradation of amplitude of oscillations of the system "plow dump-PA" and the corresponding numerical indicators shown on the right on the vertical axis. Numerical frequency values in the postprocessor window of the COMSOL Multiphysics package are displayed automatically and correspond to the maximum amplitude of PA oscillations. Analysis of the results of research suggests that the most rational location of the PA on the dump is cell C6 (Fig. 5 d), where at a frequency of 400 Hz there is an amplitude of oscillations of the system in the range $2.624 \cdot 10^{-9} - 6.847 \cdot 10^{-7}$ m.

In addition, according to the simulation results, approximate expressions of the change in the amplitude of oscillations of the system depending on the coordinates of the PA location on the plow heap were obtained. It was believed that the coordinate system is located in the lower left part of the plow blade.

$$A = a + by + cy^2 + dy^3, \tag{2}$$

where A is the oscillation amplitude of the system; x is the corresponding coordinate of the PA location on the dump ($0.1 < x < 0.2$);

$a = 7.4609 \cdot 10^{-6}$, $b = -0.00013040883$, $c = 0.000727255$, $d = -0.0012261667$ - coefficients;

$$A = f + ky + gy^2 + hy^3 + jy^4, \tag{3}$$

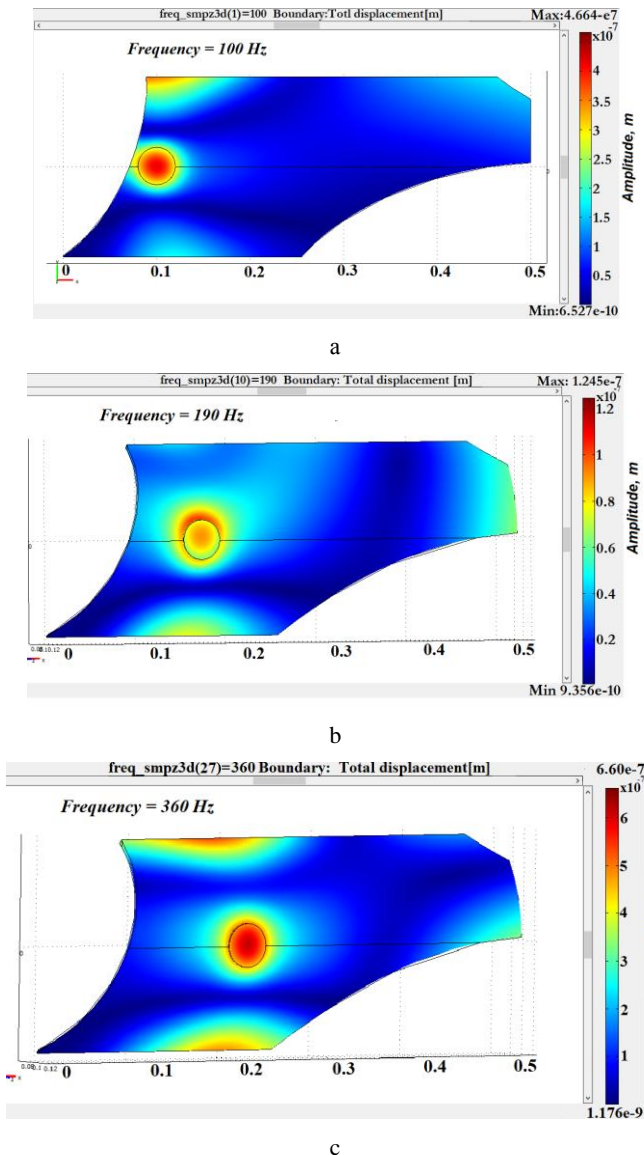
where y is the corresponding coordinate of the PA location on the dump ($0.1 < y < 0.15$),

$f = -2.00368 \cdot 10^{-5}$, $k = 0.00073820533$, $g = -0.0095278667$, $h = 0.052941867$, $j = -0.10683733$.

Conclusion

In the process of studying multiphysical processes, including electrophysical ones, the resonance frequency at which the piezoelectric actuator maximally influences the amplitude of oscillations of the plow blade and which is equal to 400 Hz. The maximum amplitude of oscillations of the "plow dump-PA" system, which is $6.847 \cdot 10^{-7}$ m, and the rational location of the piezo actuator on the heap, which provides this effect. The performed numerical experiments allowed to obtain approximation expressions for simplified determination of the amplitude of oscillations of the system depending on the coordinates of the piezo actuator placement on the heap.

The results of research can be used in the design of vibrating plows based on piezoceramic actuators.



3. References

1. R. Sh. Abakarova Regulirovanie selskogo hozyaystva. Polozhitelnyie storonyi zarubezhnogo opyita. Vestnik Irkutskogo gosudarstvennogo tehničeskogo universiteta. № 1 96. C. 129-133. (2015).
2. Ya. S. Gukov Obrobitok Gruntu. Tehnologiya i tehnika. Mehaniko-tehnologične obgruntuvannya energozberigayuchih zasobiv dlya mehanizatsiyi obrobitku Gruntu v umovah Ukraini. K.: Nora-Print, 280 c. (1999).
3. S.S. Yaschenko, S.A. Filimonov, A.V. Batrachenko Rozrahunok sil, scho vinikayut pri stvorenni vibratsiy za dopomogyu smart piezoceramics, ta doslidzhennya yih rozpodilu u pluzhnomu vidvali. Visnik Cherkaskogo derzhavnogo tehnologičnogo unIversitetu. №2. C.21-28. (2020).
4. A.E. Panich, S. Zhukov Pezoelektricheskoe priborostroenie. Pezoelektricheskie aktuatoryi. Rostov-na-Donu: SVVR, 159 c. (2008).
5. A M. Fennimore, T. D. Yuzvinsky, Wei-Qiang Han, M. S. Fuhrer, J. Cumings, A. Zettl Rotational actuators based on carbon nanotubes. Nature. V. 424. P. 408-418. (2003).
6. M. Köhler, W. Fritzsche Nanotechnology: An Introduction to Nanostructuring Techniques. Weinheim: Wiley-VCH, 272 p. (2004).
7. Yu. D. Tretyakova Nanotehnologii. Azbuka dlya vseh. M.: Fizmatlit. 368 c. (2008).
8. T. Cornelius Handbook Techniques and Applications Design Methods; Fabrication Techniques; Manufacturing Methods; Sensors and Actuators; Medical Applications. Springer, 1350 p. (2007).
9. V.M. Bulgakov, M.O. SvIren, I.P. Palamarchuk, V.V. Driga, O.M. Chernish V.V. VibratsIynI mashini sIlskogospodarskogo virobnitstva: monografiya. Kirovograd: KOD, 513 c. (2012).
10. S.S. Yaschenko S.A. Filimonov A.V. Batrachenko, N.V. Filimonova Ispolzovanie smart piezoceramics dlya obra-botki pochvyi v selskom hozyaystve. "Visnik Cherkaskogo derzhavnogo tehnologično-go universitetu" №2. C.30-36. (2019).
11. V.Ya. Halchenko, S.A. Filimonov, A.V. Batrachenko, N.V. Filimonova Increase the Efficiency of the Linear Piezoelectric Motor. J. Nano- Electron. Phys. 10 No 4, 04025 (5pp) (2018),
12. V.Ya. Halchenko, Yu.Yu. Bondarenko, S.A. Filimonov, N.V. Filimonova Determination of influence of geometric parameters of piezoceramic plate on amplitude characteristics of linear piezomotor // Electrical Engineering & Electromechanics. no.1. P. 17-22. (2019).
13. S.N. Zhukov Pezoelektricheskaya keramika: printsipyi i primeneniye: monografiya. Minsk: OOO FUAuinform, 112 c. (2003).
14. L. Spicci, M. Cati Ultrasound piezo-disk transducer model for material parameter optimization. Excerpt from the Proceedings of the COMSOL Conference. Paris, P. 1-7. (2010).
15. V. Sharapov Piezoceramic sensors. Heidelberg, Dordrecht, London, New York: Springer Verlag, 498 p. (2011).

Research of combustion engine oil quality over exploitation period

Mažeika Darius¹, Balnys Rytis¹, Kandrotaitė Janutienė Rasa¹

Faculty of Mechanical Engineering and Design – Kaunas University of Technology, Lithuania¹

E-mail: darius.mazeika@ktu.lt, raskand@ktu.lt

Abstract. Different types of oil are used widely in all over the world. It is used for lowering friction force at the contact zones, e. g., bearings, gears and other areas where at least one element is moving in relation to another one. Several types of oils find place in automotive industry: mineral, semi-synthetic and synthetic. Over the time oil characteristics were improved by enriching with different additives. Special additives can reduce friction forces, present better wash of abrasion products, extend oil life, etc.

This article deals with the research of degradation of oil lubrication quality in vehicle combustion engine over the exploitation period. Quantity of contaminating particles in oil sample was determined by optical microscopy. Oil film strength test was performed with oil samples used after various exploitation periods.

Keywords: OIL QUALITY, INTERNAL COMBUSTION ENGINE, EXPLOITATION PERIOD, OIL FILTER, CONTAMINATION PARTICLES.

1. Introduction

Automotive industry contains companies and activities involved in the manufacture of motor vehicles, including components such as engines and bodies. This industry produces transport means, that are very popular and used in all over the world. Every mechanical assembly of transport mean in order to operate smoothly, it is necessary to use lubricating liquids for lowering friction forces and increasing its lifetime. The lifetime of lubricating liquids can be increased by using additional elements: zinc dialkyl dithiophosphates, titanium, graphite, molybdenum disulfide, tungsten disulfide, polytetrafluoroethylene or chlorine [1]. Recently, lubricating liquids are of very high quality, that allows to use it for longer exploitation time. However, during exploitation time engines or gearboxes of cars, vans or trucks, fail. Inside of these mechanisms most of car services have founded motor oil of high viscosity and polluted with abrasive particles. Over the exploiting time these particles can mix with motor oil and pollute oil filter. Polluted oil filter decreases oil flow for journal bearings and increase combustion engine wear.

The problem is a common internal combustion engine damage due to insufficient, inefficient engine lubrication. Modern car manufacturers recommend oil change via intervals from 8000 km up to 60000 km. Change interval depends on the car's lubrication system design and on the filtration system. For example, Ford manufacturers recommend their car oil change every 20000 km up to 50000 km depending on the vehicle model and type of internal combustion engine. Oil and oil filters also must meet the requirements for longer distances and engine working hours. However, different car manufacturer has different specifications, for example, Nissan recommends oil change from 8000 km up to 30000 km intervals [2].

While car operates over time, the oil physical and chemical properties change, the oil loses its active ingredients, which gives additives. Aging oil usually increases its viscosity and a variety of contaminants and oil oxidation occurs due to temperature changes. Oil durability also depends on the engine design, oil tanks – sump size and the amount of oil poured into the engine lubrication system, the oil pump performance, air, oil and fuel filtration system design. So, without changing the oil on time, pollution significantly increases and the effectiveness of the active substances diminishes. If the oil is not changed in time, further consequences may occur – the rapid growth of contamination of engine parts, as well as increased mechanical and corrosive abrasion, oil filter clogging, lubricating channel blockage and other destructive processes [3].

Oil can be tested in a variety of methods, starting with contamination determination and finishing with chemical composition of used oil. Carrying out such research and in order to identify problems, it is necessary to gather information and adhere to certain set goals. In order to study the oil for some reason and to get more accurate data and results, it is necessary to determine which mode the car will be running, what oil type and filters will be used, how many kilometers or operating hours will be performed [4]. As billions of money are spent every year on replacing or

repairing faulty units due to poor or insufficient lubrication, it is appropriate to carry out studies that may help to reduce the problem. Table 1 shows the most common oil tests performed [4].

Table 1. Usually performed oil quality tests [4]

Category	Research object	Methods of analysis
Wear	Quantity size and distribution of contamination particles	Microscopy
	Particles shape	Ferrogaphy
	Metal particles	Spectroscopy of a rotating disk electrode (RDE)
Pollution	Sand and mud	Microscopy
	Unburnt fuel	Fuel Sniffer Spectro, Gas chromatography (GC)
	Water	Infrared (IR)*, Karl Fischer Titration (KF)
	Water coolant, antifreeze	Infrared (IR)
	Soot	Infrared, soot meter
Fatigue	Other liquids	
	Oxidation, nitration, sulphitization	Infrared (IR)
	Viscosity	Viscosity testers
	Acid numbers or base numbers	Titration

3. Research methodology

An optical microscope Nikon was used for studies to see solid particles inside the used oil. An objective Nikon TU Plan Fluor 20x / 0.45 A was chosen, and Nikon DS-Ri2 with a 16x megapixel camera was used to obtain images. NIS-Elements D software was used to process the images.

The Timken test is a test that meets international standards and is a test method that meets American standards (ASTM No. D 2782) [5]. A special experimental stand is used for this test (Fig. 1).

The Timken machine has an electric motor (4) that rotates the shaft (5) at 800 rpm. At the beginning of the test, the sample (2) is placed in the lever, then the oil bath (3) is filled with the oil to be analyzed and the apparatus is started. After the apparatus has been tampered with, the selected weight (2.5 kg) is placed on the lever (1) for a few seconds and the sample is further abraded for the selected time. The tests usually give a constant load and a constant wear time. After the tests, the samples are removed from the lever and further examined by other methods.

After all samples have been tested by Timken test, they are carefully analyzed visually. Filter samples were taken in three stages. The first stage, when the car travels about 25,000 kilometers, the second stage, when the maximum permissible mileage is achieved, e.g. 50,000 kilometers, and the third stage, when the car travels the maximum permissible mileage, but the filter is used only

half the range, e.g. after about 25,000 kilometers only the oil filter was replaced.



Fig. 1. The Timken test experimental setup: 1 – lever with the load, 2 – sample, 3 – oil bath, 4 – electric motor, 5 – shaft

4. Research progress

Oil samples from five different cars were collected for the study. When the car arrived for service maintenance, 40 ml of used oil was taken as a sample, which was safely placed in a sealed tube (Fig. 2). Some literature sources [6, 7] mention that the oil filter often becomes dirty faster than the oil change time comes and the oil does not longer flow through the safety valve, causing contamination increase rapidly and can cause significant damage of the engine or its components. Therefore, it was decided to collect the oil samples at a halfway of the oil change interval (~ 25000 km), without changing the oil itself, to change only the oil filter, take a sample of used oil and the used filter, and repeat this procedure after 50000 km.



Fig. 2. Tubes with samples of used oil

For testing and operation of the cars, original Ford oil was used, which meets the requirements set by the car engine manufacturer. The oil specification is given in Table 2.

Table 2. Specifications of engine oil used

Oil name	Oil type	Oil specification
Ford FORMULA F	SAE 5W-30	ACEA A5/B5 WSS-M2C913-C WSS-M2C913-B WSS-M2C913-A

This oil is suitable for most Ford cars. It is a high quality fully synthetic oil. It reduces friction of engine parts and fuel consumption, features excellent motor protection and wash quality. It ensures optimal engine start at low temperatures and reduces CO₂ emissions [8].

Timken samples (Steel grade 1010, Ø12 mm) were prepared according standard requirements [5] and used during the investigation. After placing the Timken sample on the test bench (Fig. 1), the oil bath was filled with oil. The apparatus started before any load had been applied, the load was applied to the load lever when the stand was launched and the Timken sample was further

abraded for the selected time. Figure 3 shows a Timken sample when tested for 7 minutes in a new, unused oil.



Fig. 3. Timken sample after 7 minutes of abrasion

For further tests, the abrasion time and load of the first Timken sample were set up. Accurate collecting of the results requires the same load and abrasion time that should be maintained for all Timken samples and different oil samples.

At the beginning of the tests, the Timken sample was first tested in a clean, unused oil, the wear was measured, for the purpose to have comparable results with the ones obtained for the used oil samples.

After every test, a different oil sample was changed, the oil bath was washed with a special oil and grease-washing liquid to remove unwanted impurities, as abrasion of the sample could accumulate its abrasive particles in the oil, which later could deteriorate the lubricating properties of the oil.

Fig. 4 shows scar diameter of Timken sample obtained after the test of abrasion in used oil for three different situations – I, II and III. Here is the description of the mentioned situations:

I – car mileage was about 50000 km, oil filter exploitation duration was the same;

II – car mileage was about 50000 km, oil filter was changed after each 25000 km (twice);

III – car mileage was about 25000 km, oil filter exploitation duration was the same.

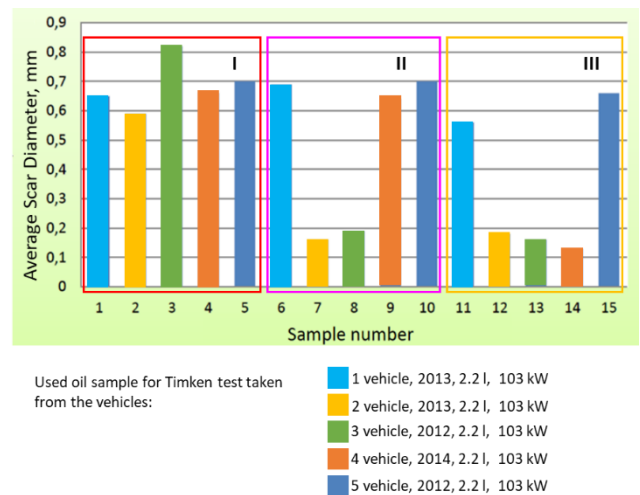


Fig. 4. Measurement of average scar diameter of Timken sample after abrasion test in oil

Determination of hard particles in oil

After all the oil samples have been collected, they were further examined under a microscope to determine how the oil contamination has changed with the number of kilometers traveled. When examining oil samples under a microscope, the focus was on hard particles and their content in the oil. After microscopic analysis of all samples, the results were compared to check for a change in oil contamination after changing the oil filter in the middle of the oil change interval.

The nature of the objects found under the microscope was assessed on the basis of similar studies already carried out, which described in detail the characteristics of every object. The scientists describe how the shape, color, surface structure and dimensions of an object can be used to partially determine what kind of material is in, as well as to decide, based on the surface profile, what kind of wear can prevail [9, 10]. Figure 5 shows the oil containing undesirable particles. Figure 6 shows the surface of an abrasion particle, showing abrasion marks, i.e., longitudinal scratches, from which it can be inferred that this particle may be a rupture of the cylinder walls or from where the slip tinnitus predominates [9, 10].

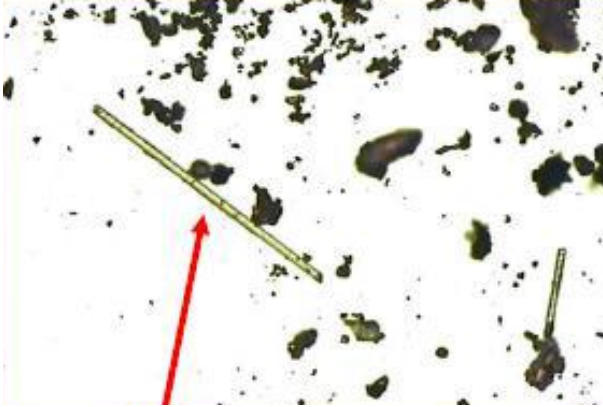


Fig. 5. Microscopic photo of used engine oil (200x) [9]



Fig. 6. Abrasion particle surface profile (1000x) [10]

The Fig. 7 and 8 show optical microscopic images oil samples taken from the first car. Particles larger than $10\mu\text{m}$ were measured and marked on the images, while other, smaller visible particles were marked with arrows during microscopic image analysis and examination of the detected particles.

Examination of the microscopic images and the particles seen in them revealed that, in terms of dimensions, the largest particles were observed in the oil samples which were taken from cars that had worked approximately 50,000 km. The dimensions of the largest particles detected in the first sample (Fig. 7) were $49\mu\text{m}$ and $45\mu\text{m}$. According to the dimensions and shape of these hard particles, based on the literature sources [10, 11], it can be stated that it could be a metal chips, which may be caused friction of parts. The particles of such size do not pass through the filter material, e.g. they are trapped by the oil filter, therefore, it can be argued that the oil filter did not filter the oil at fully, i.e., part of the oil flowed through the filter and other one flowed through the safety valve and the filter had already started to clog. Further examination of the first five samples showed that in terms of the amount of particles in the oil, most of them are visible in the third sample. Theoretically, it is normal for this oil to have the highest levels of contaminants, as this oil has been in operation for 51500 km.

Examination of oil samples 6-10 of car exploited approximately 50,000 km, but replaced the oil filter at the 25000 km, showed a difference compared to the first five samples. Slightly fewer hard particles were observed in these oil samples, and the largest particle

detected was only $20\mu\text{m}$, which was several times larger than the particles detected in the first samples.

In samples with a mileage of up to 25000 km (11-15), the observed particles are only up to $10\mu\text{m}$, compared to the first ten oil samples, these hard particles are less visible. The most noticeable feature is a soot, as well as small particles whose shape and dimensions are difficult to detect by optical microscopy.

Fig. 9 presents the number of found particles larger than $5\mu\text{m}$ per $0,36\text{mm}^2$ test oil smear area.

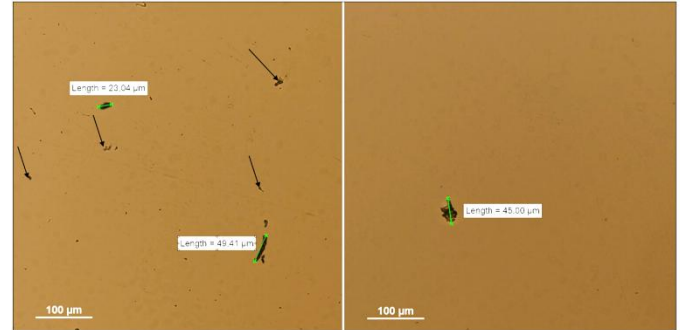


Fig. 7. Sample No. 1 after mileage of 49000 km

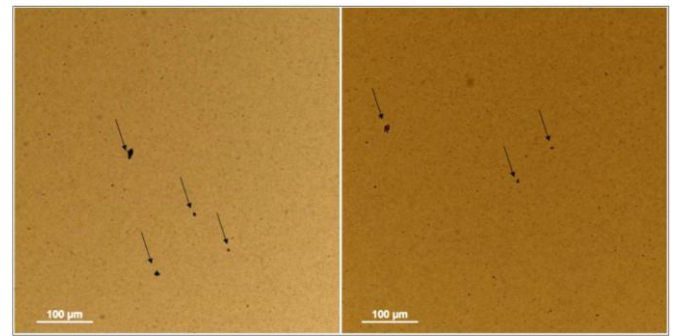


Fig. 8. Sample No. 11 after mileage of 20000 km

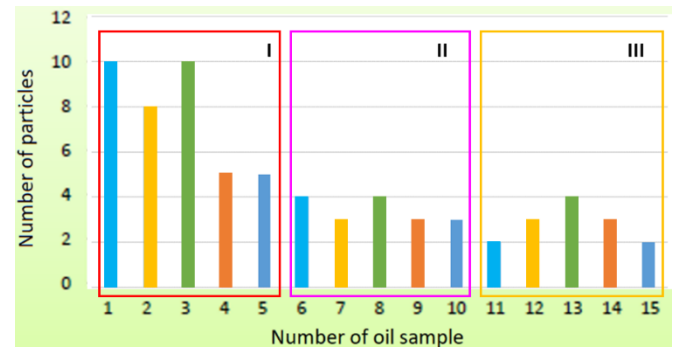


Fig. 9. Number of particles per $0,36\text{mm}^2$ area. Designation with colors is the same like in Fig. 4

5. Discussion

As technology advances but oil resources dwindle, oil and car manufacturers are increasingly striving to increase oil quality while increasing the oil change interval. It is no secret that a significant proportion of modern cars have a range of 50000 km or more. However, faults caused by insufficient lubrication are not uncommon. The question arises as to whether the oil with which the car has traveled 40000 to 50000 km can be fit for use and do not damage the engine components. We know that when operating a car in different operating modes, the oil is affected unequally, if the car is used at high loads more often, then the oil is subjected to a higher load, so it loses its lubrication properties faster. Perhaps when operating the vehicle in more severe conditions, the interval should

be shortened or measures taken to reduce oil contamination, such as changing the filters between the change intervals.

After analyzing all the oil samples in terms of mileage, the biggest contamination and biggest hard particles were found in the first five samples, where the oil life was 50000 kilometers and more. In this case, the oil was heavily contaminated, the oil filter inefficiently filtered the oil, engine components with more contaminated oil wear faster, and as a result, the contamination increased much faster than with clean oil.

After analysis, it was determined that the cleanest oil was the one that had been operating for about 25000 km, in this oil, no hard particles were observed that could pose a significant threat to the internal combustion engine assemblies. There could be stated that the oil filter and the whole filtration system filtered the oil sufficiently, the filter was not clogged and worked effectively.

After performing the experiment and changing the oil filter, in the middle of the oil change interval, after microscopic analysis, it could be seen that the particle content and dimensions were much lower than in the oil samples that served the full range. Changing the oil filter after half-termed exploitation was effective and expedient.

6. Conclusions

1. In the course of the investigation, oil samples were collected from five different cars with identical engines, and the engine oil used and the oil filters were the same in all cars. For more accurate data, cars with similar operating conditions were selected. The nature of oil contamination was determined by microscopic analysis of oil samples based on literature sources. The shape and visual appearance of the objects visible in the oil determine the nature of the particle, e.g. whether it is a metal particle, dross, dust, or something like that.

2. The oil samples contaminated mostly were determined during microscopic analysis: 1 (49000 km.), 2 (47500 km.), 3 (51500 km.), 4 (48650 km.). The biggest hard particles were observed analyzing these samples. A comparison of all the oil samples collected showed that the least contaminated samples were those with a mileage of up to 25000 km and the most contaminated were those with a mileage of about 50000 km.

3. During the oil sampling, an experiment was performed – as the aforementioned car oil change interval was 50000 km. After performing this experiment and comparing the results with the results of all the oil samples, it was observed that the oil contamination is significantly reduced when just the oil filter was changed between the oil change intervals.

4. A visual analysis of the used oil filters was performed, during which was determined that the most contaminated filter is No. 3 (51500 km.). It showed many metal wear particles and other foreign objects.

6. The Timken test revealed that the quality of the sample No. 3 (51500 km.) oil was the worst, as with this oil the Timken sample

wear out the most - 0.82 mm. Abrasions were also found to be lower when tested with oil in which only the oil filter was changed. Thus, the study showed that the quality of the oil, its lubrication properties could be improved and the contamination could be reduced when only the oil filter has been changed between oil change intervals.

7. References

1. Experimental Aircraft Info. Available in: <https://www.experimentalaircraft.info/articles/engine-lubrication-6.php>
2. 2016 Service and Maintenance Guide. Available in: <https://owners.nissanusa.com/content/techpub/common/2016/2016-nissan-service-maintenance-guide.pdf>
3. Jučas P. Exploitation Materials. Kaunas, 2007, 61-67 p.
4. Oil Analysis Handbook. Predictive Equipment Maintenance. Third Edition. Available in: <https://info.spectrosci.com/oil-analysis-handbook-download>
5. ASTM D2782-20 Standard Test Method for Measurement of Extreme-Pressure Properties of Lubricating Fluids (Timken Method).
6. OPTIMIZING OIL CHANGE INTERVALS. Available in: <https://www.macallister.com/parts-service/service-solutions/machine-fluid-analysis/optimizing-oil-change-intervals/>
7. Ewa Rostek, Maciej Babiak. The experimental analysis of engine oil degradation utilizing selected thermoanalytical methods. 13th International Scientific Conference on Sustainable, Modern and Safe Transport (TRANSCOM 2019), High Tatras, Novy Smokovec – Grand Hotel Bellevue, Slovak Republic, May 29-31, 2019. Transportation Research Procedia 40 (2019) 82–89.
8. Original Ford Motor Oil. Available in: <https://www.ford.co.uk/owner/service-and-maintenance/service-promotions/castrol-products>
9. Used Engine Oil Analysis. User Interpretation Guide 16-17p., elaborated by the CIMAC Working Group 'Marine Lubricants' in May.
10. Used Lube Oil Analysis and Analytical Ferrography. Available in: https://www.academia.edu/40653688/Used_Lube_Oil_Analysis_and_Analytical_Ferrography
11. R.K.Upadhyay. Microscopic technique to determine various wear modes of used engine oil. Journal of Microscopy and Ultrastructure Volume 1, Issue 3, December 2013, 11-114.

Kinematic analysis of the slider-crank mechanism of an internal combustion (IC) engine using modern software

Marko Lučić¹

Faculty of Mechanical Engineering, University of Montenegro, Podgorica, Montenegro¹

E-mail: marko.l@ucg.ac.m

Abstract: The subject of research in this paper is the kinematic analysis of the slider-crank mechanism of an internal combustion (IC) engine. The piston, connecting rod and crankshaft are the most important moving parts of an IC engine. The performance of IC engines largely depends on the design of the mentioned parts. Special attention should be paid to the kinematic analysis of the slider-crank mechanism, when constructing IC engines. Properly performed kinematic analysis is a prerequisite for the design of an efficient IC engine. Today, there are many software packages that make it much easier for engineers to perform fast and efficient kinematic analysis of machine assemblies. This paper presents the use of kinematic analysis software on the example of a slider-crank mechanism, an IC engine.

Keywords: IC ENGINE, PISTON, CRANKSHAFT, CONNECTING ROD, 3D MODELING

1. Introduction

In the general case, an engine is a propulsion machine that converts some kind of energy into mechanical work. Reciprocating internal combustion engines (IC engines) belong to the category of heat engines, which are used as propulsion machines in everyday use to overcome some external resistance in order to perform and perform certain work. The name heat engine refers to a group of propulsion machines in which the thermal energy developed by fuel combustion is used for the realization of mechanical work [1].

Kinematics is a field of mechanics, ie physics that takes into account only the movement of the body in space and time. So in kinematics we take into account the forces that cause movement, and we do not take into account the consequences of movement. It can be said that kinematics studies only the geometry of motion [2]. In order to check the mechanical stresses of the engine elements and solve problems such as: uniformity of operation, torsional oscillations of the crankshaft, engine balance, load and wear of the piston joints, it is necessary to analyze the forces occurring in the piston mechanism. It is necessary to clarify the formation of all forces, the law of their change during the working cycle and their effect during engine operation [3]. The use of modern software is an indispensable part of modern engineering. The use of software in design and construction significantly saves time and money, but also eliminates errors in the initial stages of product design. Some examples of the use of modern software in mechanical engineering are given in the literature [4-7]. An example of kinematic and dynamic analysis of a single-cylinder mechanism is given in [8-9].

A number of very complex problems must be solved when designing an IC engine. Some of them are: selection of the most favorable construction solution, assembly and installation of the most favorable auxiliary devices, realization of a favorable work cycle. The choice of design concept and engine type depends on typical conditions. These conditions are defined taking into account the conditions of exploitation and the general economic effect to be achieved by applying the new construction. When designing a new type of engine, one must strive to achieve such a construction that will be closer in its characteristics and even surpass modern engine designs. This implies the application of the latest advances in engine research and construction. The process of designing and manufacturing a new engine is very complex. In order to ensure quality production and achieve the given performance, the engine designer, in addition to providing correct drawings and calculations, must take an active part in all stages of prototype production, including laboratory tests to check and correct characteristics to meet design requirements. One of the basic analyzes in the construction of internal combustion engines is the kinematic analysis of the piston mechanism, which is of great importance for the proper and balanced operation of the engine as a whole [3].

2. Basic parts of the piston mechanism

2.1. Piston

The piston is the most loaded part of the engine. For its proper functioning in the IC engine, it is necessary to correctly determine the shape, dimensions and material of the piston. Therefore, for decades, the construction and production of pistons have been dealt with mainly by specialized manufacturers, who act as partners of engine manufacturers.

In operation, the piston is exposed to high mechanical and thermal loads and in these conditions it must:

- to separate the combustion space from the crankshaft housing by means of piston rings,
- to transmit gas forces on the connecting rod,
- to transfer the normal (lateral) force generated during the transmission of gas forces on the connecting rod to the cylinder,
- transfer heat from the piston head to the cylinder wall,
- in the case of two-stroke engines, control the gas exchange (switching mechanism)

In order to meet the above requirements, the piston must have the following properties:

- the mass of the piston must be as small as possible, so that its force of inertia is as small as possible (increases with the square of the angular velocity) at higher angular velocities.
- the stiffness of the piston face must be high, in the area of the shaft bearing as low as possible, and the piston body must be elastic.
- piston grooves must have high strength, so that the links do not damage them.
- the strength must be high even at elevated temperatures, especially in the area of the piston face.
- the piston material must have good thermal conductivity so that the temperature differences on the piston are as small as possible and so that the heat dissipation to the cylinder is as good as possible.

The piston must be designed so that it stretches as much as possible with increasing temperature, so that the gap between the piston and the cylinder is as small as possible even in the cold state, because then the sealing is better and the noise is less [10].

Pistons must meet a number of different requirements, so the material from which the pistons are made must have [11]:

- low specific gravity (due to inertia),
- high strength, (even at high temperatures),
- good thermal conductivity,
- low thermal expansion,
- low coefficient of friction,
- high wear resistance.

Figure 1 shows the piston.



Fig. 1 Piston for Diesel truck engine [10]

2.2. Piston rings

The basic tasks of piston rings are:

- sealing of the combustion chamber,
 - participation in heat dissipation from the piston to the cylinder wall,
 - regulation of oil film for lubrication.
- These requirements are performed by piston rings:
- adhering with the outer (working) surface to the cylinder wall with a certain pressure,
 - impact bearing on the side surfaces of the groove due to axial acceleration under the action of gas forces, friction forces and its own inertial force [10].

2.3. Piston pin with fuses

The basic task of the piston pin is to make the articulated connection of the piston and the connecting rod. The piston pin with the piston is shown in Figure 2.



Fig. 2 Piston pin with piston [10]

When the piston pin is in a loose bearing, it must be prevented from moving and damaging the cylinder walls. This is achieved by radial steel rings (Seeger ring or spring wire ring. For easier assembly, the Seeger ring has eyelets and the spring ring has hooked ends) [11].

2.4. Connecting rod

The connecting rod is the element that connects the piston and the crankshaft and converts a straight line into a circular motion. The connecting rod transmits the force from the piston to the crankshaft which converts the force into torque. Due to the great responsibility of the connecting rod in the operation of the engine, high rigidity must be ensured with a minimum weight of the same.

In the operation of the engine on the connecting rod operate:

- pressure forces in the longitudinal direction due to the action of combustion gases on the piston head,
- dynamic stresses due to inertial forces due to changes in velocity,
- bending forces due to piston rod movement.

The connecting rod is shown in Figure 3.



Fig. 3 Mercedes-Benz diesel engine connecting rod [10]

2.5. Crankshaft

The crankshaft transmits torque and is one of the most responsible, complex, stressful and expensive engine parts. The following requirements must be met for the crankshaft to function properly:

- there must be sufficient safety to prevent fatigue of the entire working space,
- there must be no large amplitudes of torsional, bending and axial oscillations,
- the inertial load must be brought to a reasonable level,
- crankshaft deformations must be kept to a minimum reasonable level.

The tasks of the crankshaft are:

- to convert uneven rectilinear motion into rotation,
- to convert the connecting rod force into torque,
- to transfer most of the torque to the coupling via the flywheel
- to deliver a small part of the torque to the assemblies (distribution mechanism, ignition distributor, fuel and coolant pump, fan, alternator).

The crankshaft must accelerate and decelerate the pistons and connecting rods in each stroke, so large forces of inertia act on the crankshaft [11].

Figure 4 shows the crankshaft.



Fig. 4 Crankshaft of a four-stroke diesel engine [10]

3. Kinematics of axial piston mechanism

The piston engine mechanism is used to convert the rectilinear oscillatory movement of the piston in the cylinder into the rotational movement of the crankshaft by means of a connecting rod that performs a balancing movement. This kinematic circuit allows the work on the piston, which results from the development of the operating cycle, to be obtained in the form of torque on the engine shaft. A engine mechanism consisting only of a piston, connecting rod and crankshaft is called a simple engine mechanism. With a complex engine mechanism, several elements are involved in the

transmission of movement from the piston to the crankshaft. At a certain stationary velocity mode of operation of the engine, it can be considered that the angular velocity of the crankshaft is constant, since it is maintained within the flywheel within a very narrow range. In this case the knee angle of the crankshaft is given by the expression:

$$\alpha = \omega t \text{ (rad)} = \frac{180}{\pi} \cdot \frac{\pi n}{30} t \text{ (degree of crankshaft)} \quad (1)$$

The angle of the crankshaft is given as a function of time only, so all kinematic quantities, ie. path, velocity and acceleration can only be expressed as a function of the crankshaft angle, ie time t [3].

3.1. Piston path

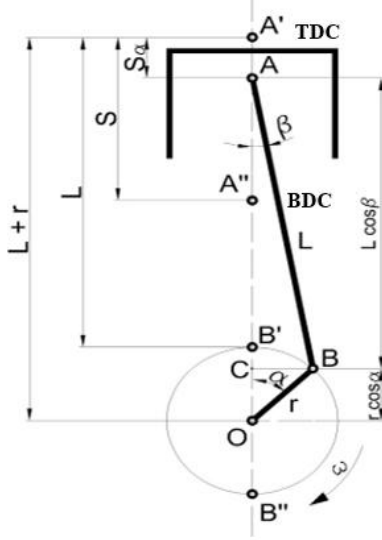


Fig. 5 Schematic representation of the piston mechanism [6]

Basic structural dimensions from Figure 3.1. are:

r - radius of the crankshaft knee,

L - connecting rod length,

$\lambda = r / L$ - dimensionless constructive characteristic of the curving mechanism,

$S = 2 \cdot r$ - piston stroke,

A' - top dead center (TDC),

A'' - bottom dead center (BDC),

α - crankshaft rotation angle,

O - crankshaft rotation axis,

B - axis of the flying crankshaft arm,

A - axis of the piston group shaft,

ω - angular velocity of the crankshaft.

According to Figure 5, the path of the piston S_a that it crossed from the external dead center is:

$$S_a = A'O - AC - CO = L + r - L \cos \beta - r \cos \alpha. \quad (2)$$

From the triangle ABO, by the sine rule we have:

$$\frac{L}{\sin \alpha} = \frac{r}{\sin \beta}, \quad (3)$$

and from here:

$$\sin \beta = \frac{r}{L} \sin \alpha = \lambda \sin \alpha. \quad (4)$$

Using the known trigonometric relationship:

$$\sin^2 \beta + \cos^2 \beta = 1, \quad (5)$$

we will have:

$$\cos \beta = \sqrt{1 - \sin^2 \beta} = \sqrt{1 - \lambda^2 \sin^2 \alpha}. \quad (6)$$

Developing this expression in Taylor's order we get:

$$\cos \beta \approx 1 - \frac{1}{2} \lambda^2 \sin^2 \alpha - \frac{1}{8} \lambda^4 \sin^4 \alpha - \frac{1}{16} \lambda^6 \sin^6 \alpha - \dots \quad (7)$$

Substituting the expression for $\cos \beta$ in equation (2) we get after arranging:

$$S_a \approx r \left(1 - \cos \alpha + \frac{1}{2} \lambda \sin^2 \alpha + \frac{1}{8} \lambda^3 \sin^4 \alpha - \frac{1}{16} \lambda^5 \sin^6 \alpha + \dots \right). \quad (8)$$

As the values of the kinematic characteristic ($\lambda = r / L$) are relatively small, only the first four terms of the previous equation can be retained without major error, so that the approximate expression is obtained for the piston path:

$$S_a \approx r \left(1 - \cos \alpha + \frac{\lambda}{2} \sin^2 \alpha \right). \quad (9)$$

Introducing replacement:

$$\sin^2 \alpha = \frac{1 - \cos 2\alpha}{2}, \quad (10)$$

we get:

$$S_a \approx r \left[1 - \cos \alpha + \frac{1}{4} \lambda (1 - \cos 2\alpha) \right], \quad (11)$$

or:

$$S_a \approx r(1 - \cos \alpha) + \frac{r\lambda}{4} (1 - \cos 2\alpha) = S_{I\alpha} + S_{II\alpha}. \quad (12)$$

The last expression allows the construction to be curved $S_{I\alpha} = r(1 - \cos \alpha)$ and $S_{II\alpha} = \frac{r\lambda}{4}(1 - \cos 2\alpha)$ and by their graphical addition, the law of change of the piston path as a function of the angle of the crankshaft knee is obtained graphically [3].

The path of the piston is not a simple harmonic function, but a complex harmonic function composed of at least two harmonics, ie two simple trigonometric functions. The first part has a significant amplitude r and a frequency identical to the crankshaft velocity. The second part has a significantly smaller amplitude $r\lambda / 4$ (about sixteen times smaller), and twice the frequency of change. Higher harmonics, which have an even higher frequency, can be neglected because they have an extremely small amplitude [1].

The change of the piston path of the first and second row as well as the total path of the piston for, for one full revolution of the crankshaft is shown in Figure 6.

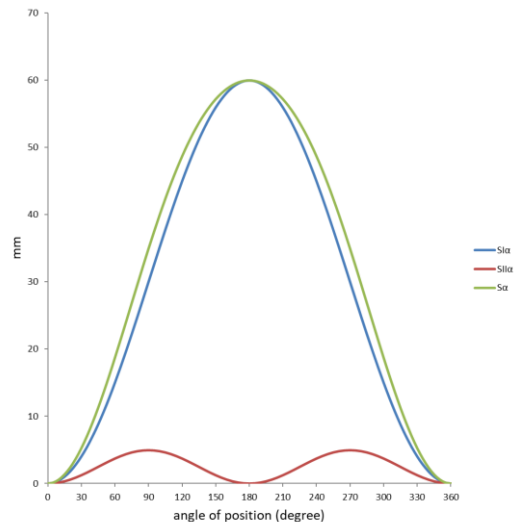


Fig. 6 Piston path [6]

3.2. Piston velocity

By differentiating the path of the piston by time, the velocity of the piston is obtained:

$$V_{\alpha} = \frac{dS_{\alpha}}{dt} = \frac{dS_{\alpha}}{d\alpha} \cdot \frac{d\alpha}{dt} = \dot{S}_{\alpha} \cdot \omega \quad (13)$$

By differentiating the expression for the piston path and including the found value S_{α}' in the previous expression, the following is obtained:

$$V_{\alpha} = S_{\alpha}' \omega = r\omega \left[\sin\alpha + \left(\frac{\lambda}{2} + \frac{\lambda^3}{8} + \frac{15\lambda^5}{256} \right) \sin 2\alpha - \left(\frac{\lambda^3}{16} + \frac{3\lambda^5}{256} \sin 6\alpha \right) \right]. \quad (14)$$

If only members that do not contain the ratio λ at higher degrees are retained, an approximate pattern for piston velocity is obtained:

$$V_{\alpha} \approx r\omega \left(\sin\alpha + \frac{\lambda}{2} \sin 2\alpha \right) = r\omega \sin\alpha + r\omega \frac{\lambda}{2} \sin 2\alpha = V_{I\alpha} + V_{II\alpha}. \quad (15)$$

By constructing the curves $V_{I\alpha} = r\omega \sin\alpha$ and $V_{II\alpha} = r\omega \frac{\lambda}{2} \sin 2\alpha$ and summing them, the law of change of piston velocity as a function of the crankshaft angle is obtained graphically [1, 3, 10].

Piston velocity is also a complex harmonic function, with the first harmonic having a significant amplitude and frequency equal to the crankshaft velocity, while the second harmonic has a smaller amplitude (about eight times) and twice the frequency [1]. The change of piston velocity of the first and second row, as well as the total piston velocity for one full turn of the crankshaft is shown in Figure 7.

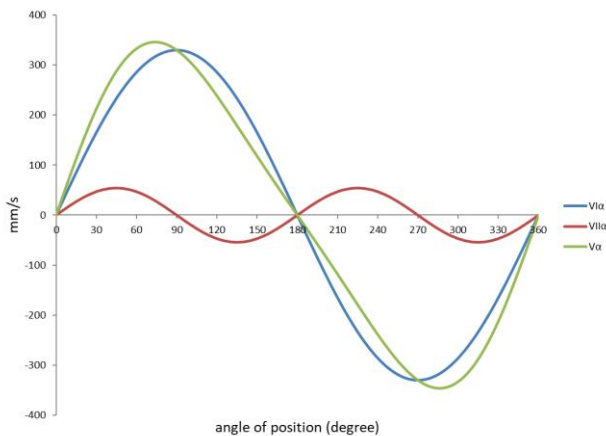


Fig. 7 Piston velocity [6]

3.3. Piston acceleration

Piston acceleration is obtained by differentiating the expression for velocity over time:

$$a_{\alpha} = \frac{dV_{\alpha}}{dt} = \frac{dV_{\alpha}}{d\alpha} \cdot \frac{d\alpha}{dt} = \dot{V}_{\alpha} \cdot \omega. \quad (16)$$

By differentiating the expression for the piston velocity or by double differentiating the expression for the piston path and including the found value in the previous expression, the following is obtained:

$$a_{\alpha} = r\omega^2 \left[\cos\alpha + \left(\lambda + \frac{\lambda^3}{4} + \frac{15\lambda^5}{128} \right) \cos 2\alpha - \left(\frac{\lambda^3}{4} + \frac{3\lambda^5}{16} \right) \cos 4\alpha + \frac{9\lambda^5}{128} \cos 6\alpha \right]. \quad (17)$$

Ignoring terms containing λ to a power greater than 1, we obtain a simplified expression for piston acceleration in the form:

$$a_{\alpha} = r\omega^2 (\cos\alpha + \lambda \cos 2\alpha) = r\omega^2 \cos\alpha + r\omega^2 \lambda \cos 2\alpha = a_{I\alpha} + a_{II\alpha}. \quad (18)$$

By constructing the curves $a_{I\alpha} = r\omega^2 \cos\alpha$ and $a_{II\alpha} = r\omega^2 \lambda \cos 2\alpha$ and their graphical addition, we obtain the law of change of piston

acceleration as a function of changing the knee angle of the crankshaft [1, 3, 10].

Piston acceleration is also a complex harmonic function, with the first harmonic having a significant amplitude and crankshaft frequency, while the second harmonic has a smaller amplitude (about four times smaller) and twice the frequency [1].

Change in piston acceleration of the first and second rows, as well as the total piston acceleration for one full crankshaft revolution is given in Figure 8.

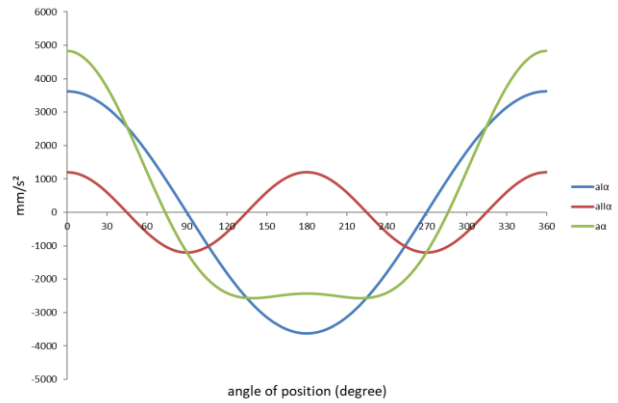


Fig. 8 Piston acceleration [6]

3.4. Connecting rod kinematics

The connecting rod performs a complex movement in a plane perpendicular to the longitudinal axis of the crankshaft, with point A (Figure 3.1) corresponding to the axis of the piston shaft, makes a rectilinear oscillatory movement along the axis of the cylinder, while point B, corresponding to the axis of the crankshaft arm, rotates evenly along the trajectory of the knee sleeve axis.

The angle of rotation of the connecting rod in relation to the axis of the cylinder is obtained from relation (3):

$$\beta_{\alpha} = \arcsin(\lambda \sin\alpha). \quad (19)$$

The maximum rotation of the connecting rod is at angles $\alpha = 90^{\circ}$ and $\alpha = 270^{\circ}$:

$$\beta_{max} = \arcsin\lambda. \quad (20)$$

The angular velocity of rotation of the connecting rod is:

$$\omega_{cr} = \frac{d\beta_{\alpha}}{dt} = \frac{d\beta_{\alpha}}{d\alpha} \cdot \frac{d\alpha}{dt} = \omega \frac{d\beta_{\alpha}}{d\alpha} \quad (21)$$

By differentiating expressions:

$$\sin\beta = \lambda \sin\alpha, \quad (22)$$

we get:

$$\cos\beta d\beta = \lambda \cos\alpha d\alpha, \quad (23)$$

and from here:

$$\frac{d\beta}{d\alpha} = \lambda \frac{\cos\alpha}{\cos\beta}. \quad (24)$$

Substituting this value into the previous expression for ω_{cr} we have:

$$\omega_{cr} = \omega \lambda \frac{\cos\alpha}{\cos\beta} = \frac{\omega \lambda \cos\alpha}{\sqrt{1 - \lambda^2 \sin^2\alpha}} \approx \omega \lambda \cos\alpha. \quad (25)$$

The maximum value of the angular velocity of the connecting rod is obtained at $\alpha = 0^\circ$ and $\alpha = 180^\circ$:

$$\omega_{cr\ max} = \pm\omega\lambda. \tag{26}$$

By differentiating the angular velocity of the connecting rod over time, we find its angular acceleration:

$$\varepsilon_{cr} = \frac{d\omega_{cr}}{dt} = \frac{d\omega_{cr}}{d\alpha} \cdot \frac{d\alpha}{dt} \approx -\omega^2\lambda\sin\alpha. \tag{27}$$

The maximum angular acceleration of the connecting rod is at $\alpha = 90^\circ$ and $\alpha = 270^\circ$:

$$\varepsilon_{cr\ max} = \pm \frac{\omega^2\lambda}{\sqrt{1-\lambda^2}}. \tag{28}$$

Figures 9 and 10 show of the angular velocity of the connecting rod and the angular acceleration of the connecting rod.

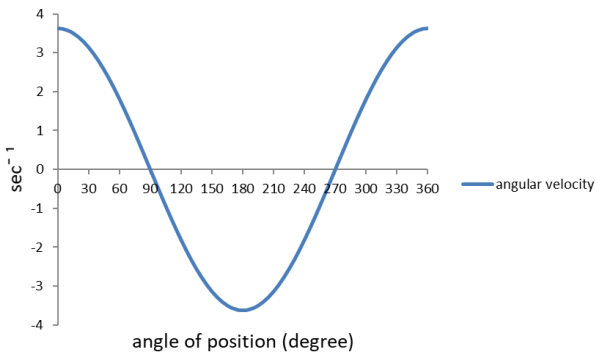


Fig. 9 Connecting rod angular velocity [6]

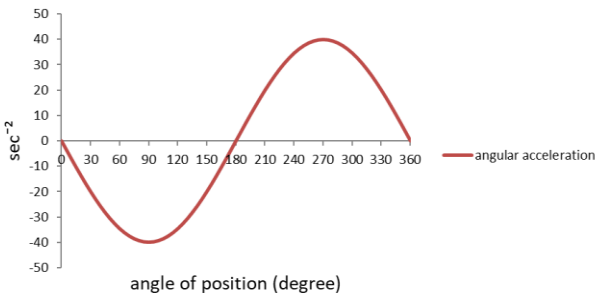


Fig. 10 Angular acceleration of the connecting rod [6]

The angular velocity and angular acceleration of the connecting rod can be shown in the common chart as shown in Figure 11.

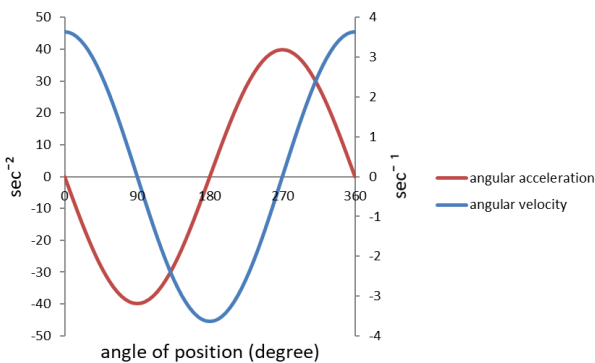


Fig. 11 Angular velocity and angular acceleration of the connecting rod [6]

An approximate expression for the calculation of the connecting rod angular velocity can be written as:

$$\omega_{cr} = \lambda\omega \left[\left(1 + \frac{1}{8}\lambda^2 \right) \cos\alpha - \frac{1}{8}\lambda^2 \cos 3\alpha \right]. \tag{29}$$

An approximate expression for the calculation of the piston angular acceleration is:

$$\varepsilon_{cr} = -\lambda\omega^2 \left[\left(1 + \frac{1}{8}\lambda^2 \right) \sin\alpha - \frac{3}{8}\lambda^2 \sin 3\alpha \right]. \tag{30}$$

4. Kinematic analysis of piston axial mechanism using CATIA software package

4.1. Piston mechanism modeling

In order to perform a kinematic analysis of the piston mechanism, it is necessary to first create a CAD model of the complete mechanism. The creation of the CAD model was done in the CATIA software package. CAD models were created: piston, piston shafts, connecting rod, crankshaft and cylinder with crankshaft bearings. Figure 12 shows CAD models of the mentioned parts of the IC engine.

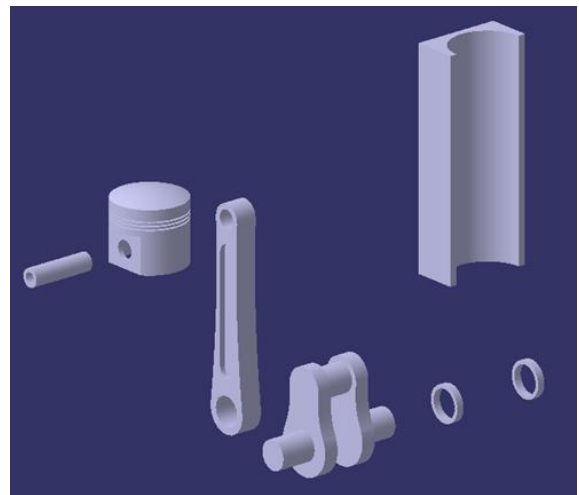


Fig. 12 View of all 5 CAD models

Figure 13 shows the assembly of the mechanism (with the indicated edges of the created parts) for which the kinematic analysis will be performed.

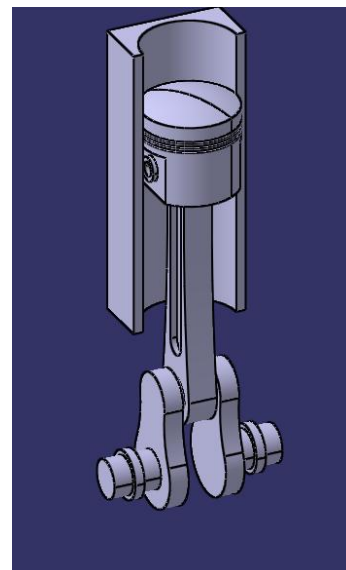


Fig. 13 View of the created CAD model

4.2. Kinematic analysis of the piston mechanism

In order to perform a kinematic analysis, it is necessary to define the appropriate boundary conditions of the assembly. The piston performs a rectilinear oscillatory movement, the crankshaft a rotational movement, while the piston rod performs a complex movement. It is necessary to define the law of movement of the mechanism, as the angular velocity of the crankshaft. In this case, the crankshaft angular velocity is set at 10 rpm. After defining the boundary conditions, the simulation of movement in a engine with a constant angular velocity of the crankshaft begins. After this, piston kinematics charts were generated. The kinematic analysis of the piston is given through the charts of path traveled, velocity and acceleration shown in Figures 14 to 16.

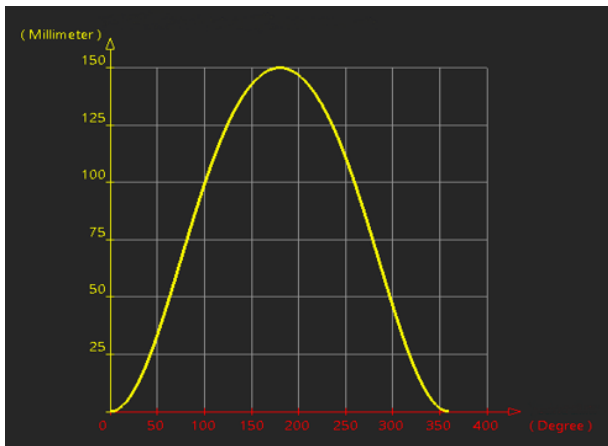


Fig. 14 Dependence of the piston path on the angle of rotation of the crankshaft for one revolution of the crankshaft

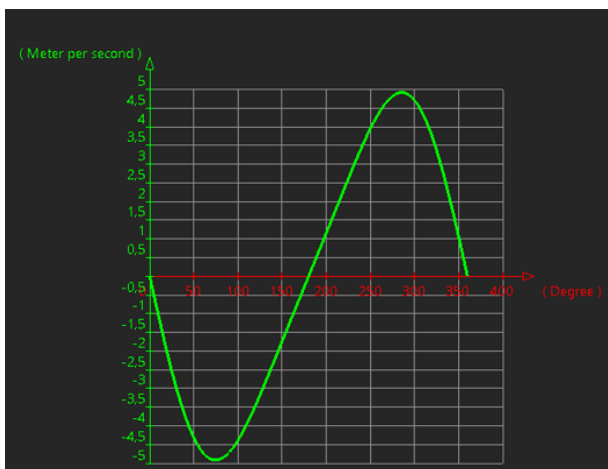


Fig. 15 Dependence of the piston velocity on the angle of rotation of the crankshaft for one revolution of the crankshaft

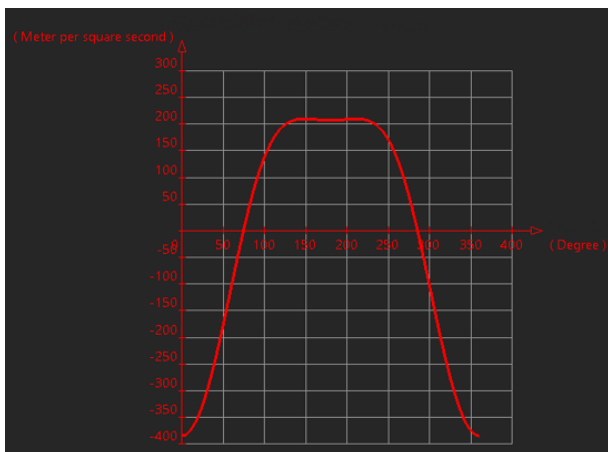


Fig. 16 Dependence of the piston acceleration on the angle of rotation of the crankshaft for one revolution of the crankshaft

Figures 17 to 19 show charts of the path traveled, the velocity and acceleration of the piston as a function of time for ten full revolutions of the crankshaft.

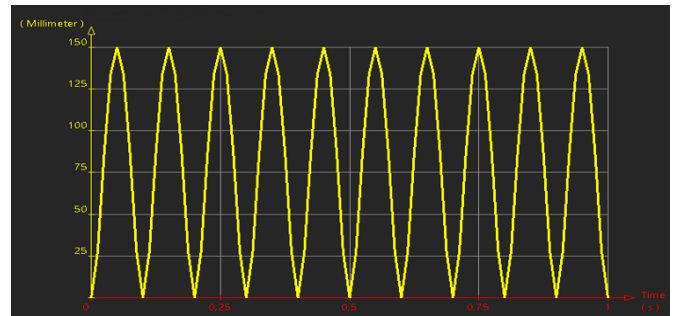


Fig. 17 Time-dependent Piston path for ten full crankshaft revolutions

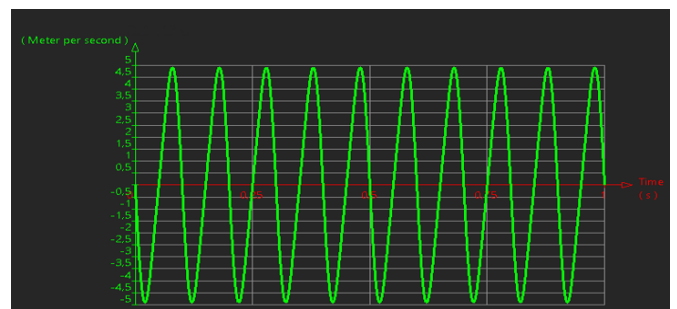


Fig. 18 Time-dependent piston velocity for ten full crankshaft revolutions

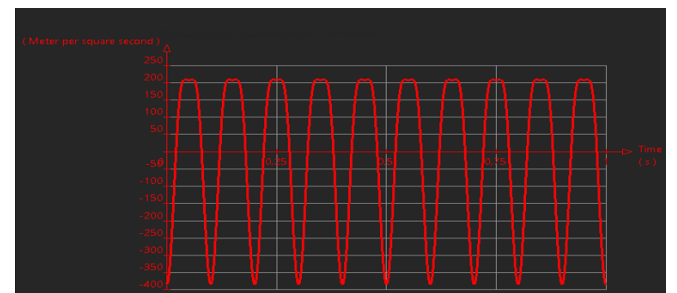


Fig. 19 Time-dependent piston acceleration for ten full crankshaft revolutions

5. Conclusion

In this paper, the path, velocity and acceleration of the piston are calculated by software, depending on the time and depending on the angle of rotation of the crankshaft. The paper also presents a detailed theoretical kinematic analysis of the piston mechanism. During the kinematic analysis of the piston mechanism, the structural appearance of the parts for which the CAD model was made is not important, only the kinematic characteristic (λ) is important, ie the length of the connecting rod and the radius of the crankshaft. Considering that the same values would be obtained when kinematic calculation in other software such as Excel, which does not require the preparation of CAD models, would significantly reduce the time spent on kinematic analysis. However, the simulation of piston, connecting rod and crankshaft movement offered by CATIA is very interesting. Further research could take place in several directions. First of all, kinematic analysis of the deaxial mechanism should be performed. Since kinematic analysis is practically an introductory analysis for dynamic piston mechanism analysis, it is simply imposed that further research be related to dynamic piston mechanism analysis. One of the further researches could be engine balancing problems, as well as the analysis of crankshaft oscillations.

6. References

1. M. Tomić i Z. Petrović, *Motori sa unutrašnjim sagorijevanjem*, Beograd, (2000)
2. K. Russell, et al., *Kinematics and Dynamics of Mechanical Systems*, Second Edition: Implementation in MATLAB and SimMechanics, Second edition, Taylor & Francis, (2018)
3. M. Živković, *Motori sa unutrašnjim sagorijevanjem, II deo*, Mašinski fakultet, Univerzitet u Beogradu, Beograd, (1980)
4. M. Burić, et al., NUMERICAL CALCULATION OF THE A6 BIFURCATION IN C3 PIPELINE IN HPP „PERUĆICA“, *Machine Design* 10(1):7-10, (2018)
5. M. Burić, et al., Calculation and analysis of the stress and deformation of crane rail clips, XXIII International Conference on Material Handling, Constructions and Logistics (MHCL 2019), Vienna University of Technology (TU Wien), Vienna, (2019)
6. M. Lučić, Kinematic analysis of piston mechanism using CATIA software package, Bachelor final thesis, University of Montenegro, Podgorica, (2016)
7. M. Lučić, Modeling and optimization of the air intake system of a Formula SAE car-Master thesis, University of Montenegro, Faculty of Mechanical Engineering, Podgorica, (2019)
8. Ikpe Aniekan Essienubong, Design Analysis of Reciprocating Piston for Single Cylinder Internal Combustion Engine, *INTERNATIONAL JOURNAL OF AUTOMOTIVE SCIENCE AND TECHNOLOGY*, VOL. 4, NO: 2, 30-39, (2020)
9. H. D. Desai, Computer Aided Kinematic and Dynamic Analysis of a Horizontal Slider Crank Mechanism Used For Single-Cylinder Four Stroke Internal Combustion Engine, *Proceedings of the World Congress on Engineering 2009 Vol II*, London, (2009)
10. Ivan Mohalac, et al., *Konstrukcije motora*, Zagreb, (2015)
11. R. Fischer, et al., *Fachkunde Kraftfahrzeugtechnik*, Verlag Europa-Lehrmittel, Nourney, Vollmer GmbH & Co. KG, 42781 Haan-Gruiten, Allemagne

Identifying Photovoltaic Water Pumping (PVWP) Systems Opportunities in Albanian's Agriculture Context.

^aIlirian Konomi, ^bLorenc Malka, ^aErmonela Rrapaj

^aDepartment of Hydraulics & Hydrotechnics, Faculty of Civil Engineering, Polytechnic University of Tirana, Albania

^bDepartment of Energy, Faculty of Mechanical Engineering, Polytechnic University of Tirana, Albania
ikonomi64@gmail.com, lmalka@fim.edu.al

Abstract: A lot of economic analyses have been conducted in the last ten years to establish the most cost-effective solution for irrigation and evaluation of the project profitability. The benefits generated by the PVWP providing water by a submersible pump located inside a deep well have been highlighted for Divjaka region. The solar potential in the site is quite enough to be used to pump water from the deep well into the tank positioned at an effective altitude which can provide the water quantity and pressure by gravity. The study shows that installing a PVWP system represents the best technical and economic solution to drive a water pump that provides water for sprinkler irrigation. The economic benefits have been also addressed, evaluating the energy production and distribution throughout the year and the specific cost per m^3 of water supplied ($\text{€}/m^3$). Renewables are the key to enhance food and water security, drive agri-food productivity, leading to socio-economic benefits in recovering from post-Covid-19. By combining our knowledge, data collected, surveys together can contribute to economic growth of our community-ensuring access to clean and affordable energy and raising the standard of living of rural and most vulnerable communities. In the area there are used two types of water pumping for irrigation purposes: Diesel driven water pumps and electricity powered water pumps. Both systems are very costly due to the high fuel cost and on the other hand self-investment to bring electricity from the national distribution lines are needed.

Keywords: PVWP, PVsyst, RES, Irrigation

1. Introduction

The development of renewable energy sources as a means of meeting the global energy demand and simultaneously replacing fossil fuels as one of the key drivers of climate change has become one of the major societal challenges of our time. In this context, photovoltaic (PV) systems offer great potential and are considered even more efficient in capturing sunlight energy than photosynthesis [1]. Energy and agri-food systems are deeply connected, and it is needed at every stage of agri-food systems, its current use in their development is unsustainable. On the other hand, about 30% of the world's energy is consumed within agri-food systems, mainly in the form of fossil fuels, and this energy is responsible for a third of their greenhouse gas emissions [2]. Renewable Energy Sources is essential for agri-food systems transformation and development, climate resilience and net-zero strategies by 2030 in Albanian context as the majority of the rural population lies their economy on agriculture. Over 2.5 billion people worldwide rely on agriculture for their livelihoods making the sector a key driver for development. These findings are becoming even more relevant, as water demand for irrigation is expected to increase in prospective future climatic conditions [3-4]. Hence, a properly and well-designed irrigation system addresses uniform water application quantities in a timely manner while minimizing losses and damage to soil and crops as well. The design of a proposed gravity sprinkler irrigation system will smooth water characteristics and application rates in respect to the demand and the right time.

In the other hand physical characteristics of the area to be irrigated must be considered in locating the lines and spacing the sprinklers or emitters, and in selecting the type of mechanized system.

The location of the water supply, capacity, and the source of water will affect the size of the pipelines, irrigation system flow rates, and the size and type of pumping plant to be used. The power unit selected will be determined by the overall pumping requirements and the energy source available. The use of PVWP technology for irrigation is considered an innovative and sustainable solution with the aim to provide cost-effective solution within off grid PV concept. Such systems can promote the use of agriculture land, especially in remote areas of Albania.

The combination of PVWP technology with water saving irrigation techniques and sustainable management of the groundwater resources can lead to several benefits. From the technical point of view this system can offer the improvement of grid reliability and limitation of power outages, protection of critical loads, independence from national grid supply, and increased energy security coupled with a fixed energy cost which is immune to future tariffs and fossil fuel costs increases. This article presents a real

application “**Photo Voltaic Water Pump**” (PVWP) installed in Divjaka region to provide water for irrigation 2.0 ha.

2. Off - Grid PV systems applications

Solar irrigation, among the most mature applications, is being widely adopted to improve access to water, thus enabling multiple cropping cycles and increasing resilience to changing rainfall patterns. The use of solar irrigation pumps has raised farmers' incomes by 50% or more in India compared to rain-fed irrigation. In Rwanda, smallholder farmers' yields have grown by about a third. The use of solar irrigation also displaces current and future fossil fuel use as the land area under irrigation expands. In so doing, it lowers emissions. Bangladesh's Nationally Determined Contribution under the Paris Agreement, for example, identifies solar irrigation as a key measure to mitigate climate change. Life-cycle emissions for solar-powered water pumping are estimated to be 95% to 98% lower than for pumps powered by grid electricity or diesel fuel [5]. Today, PV is one of the fastest-growing renewable energy technologies and is ready to play a major role in the future global electricity generation mix and a contribution for some 3.8 million jobs, or nearly a third of the sector total [6.]. Using solar PV to power mini-grids is an excellent way to bring electricity access to people who do not live near power transmission lines, particularly in developing countries with excellent solar energy resources and reducing the negative effect on environmental.

The cost of manufacturing solar panels has plummeted dramatically in the last decade, making them not only affordable but often the cheapest form to be replaced and integrated in existing power systems. Solar panels have a lifespan of roughly 30 years and come in variety of shades depending on the type of material used in manufacturing.

Off grid PVWP systems applications have been studied to cover a lot of issues, especially to provide water for drinking purposes in the areas that suffer the lack of electricity. Nevertheless, the drastic fall in prices of PV modules due to the new-born production and costless technologies of the PV lead to increased interest on research and development of off grid PV systems, encouraging greater system flexibility and large-scale integration and new applications especially in Albania. It is also essential to identify economic, technical, and environmental constraints that can negatively affect the 3 operations of PVWP systems.

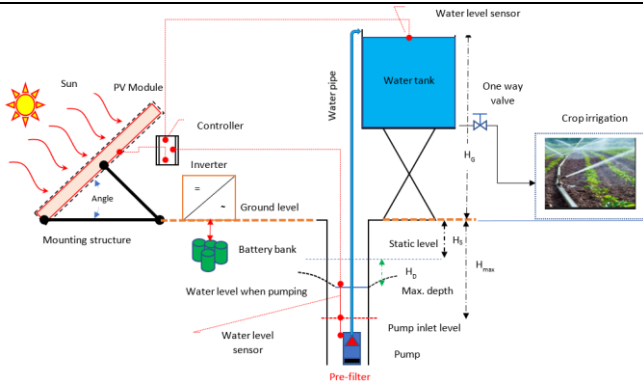


Figure 1: Integrated proposed PVWP system.

Both systems can be applied using open or under pressure water tank. The pump can be immersed or on the ground level. The water is pumped into a storage tank, according to sun availability. Pressure (head) is mainly related to the difference between the input and output levels. The pump should at least provide a total head which as a result of several contributions. In PVsyst the ground level served as a reference, hence:

where:

H_G =head due to the height of the outlet pipe above the ground (assuming that outlet pressure is negligible).

H_S =static head due to the depth of the water level in the well, in absence of any pumping.

H_D = dynamic "drawdown" head: in a borehole well, the effective water level is dynamically lowered by the water flow extraction

H_F =friction losses in the piping circuit, which depend on the flowrate. Solar PV offers better benefits and reliable solutions for consumers in rural areas who do not have access to the grid [7]. The economic benefit is assessed based on the LCOE which represents a good starting point to compare benefits and competitiveness of different technologies. Photovoltaic systems are cost-effective in small off-grid applications, providing power, to rural homes in developing countries, off-grid cottages and motor homes in industrialised countries, and remote telecommunications, monitoring and control systems worldwide.

The studies have demonstrated that a solar PV combined with diesel engine (hybrid) has relatively lower LCOE than a pure diesel generator-only. The IEA estimates that to achieve the goal of universal electricity access, 70% of the rural areas that currently lack electricity will need to be connected using mini grid or off-grid solutions. Photovoltaic systems can be combined with fossil fuel driven (Genset) motors. Off-grid applications include both stand-alone systems, and hybrid systems, which are similar to stand-alone systems but also include a fossil fuel generator (Genset) to meet some of the load requirements and provide higher reliability. The studies have demonstrated that a solar PV combined with diesel engine (hybrid) has relatively lower LCOE than a pure diesel generator-only. Nevertheless, the capital cost of the battery, which is one of the most significant components in LCOE evaluation aims to be reduced to more than 60% by 2030 [8]

3. Photovoltaic theory and PVWP calculations.

In this paper the off-grid applicability of the PVWP project altering the existing genset/electric water pump options is investigated for irrigation. Thus, an accurate methodology comprehending in-depth analysis of the benefits must be applied and always required. The need for a pile of datas including physical characteristics, financial viability, environmental advantage, carbon credits, social or other self-interests of the project, will help the energy planners to a mature decision. For this work PVsyst model is chosen. The model uses a computerized system with integrated mathematical algorithms and top to bottom approach. It provides a cost technical and economic analysis and also some financial summary. The PVsyst Software

has been developed to overcome the barriers to clean energy technology implementation at the preliminary feasibility stage.

First it is analysed the capacity and structure of the actual water demand and then choosing the right PVWP system. For the chosen water demand and pumping water system it is easy to select from the database the most suitable module type and model, respectively matching on recommendations and trends. The water is provided from surveys in the site, from the literature of the field from recommendations and also from the owner declarations.

4. Basics of Solar Energy Theory

Before entering into the details of the PV model, it will be useful to review briefly some basic concepts of solar energy engineering. Many of the variables derived in this section will be used in several parts of the model. For the most part, the equations in this section come from a standard textbook on the subject, Solar Engineering of Thermal Processes, by Duffie and Beckman (1991) [9], to which the researchers can address various technical aspects.

5. Declination

The declination is the angular position of the sun at solar noon, with respect to the plane of the equator. Its value in degrees is given by Cooper's equation:

$$\delta = 23.45 \sin \left(2\pi \frac{284 + n}{365} \right) \quad (2)$$

where n is the day of year (i.e. $n=1$ for January 1, $n=32$ for February 1, etc.). Declination varies between -23.45° on December 21 and $+23.45^\circ$ on June 21.

6. Solar hour angle and sunset hour angle

The solar hour angle is the angular displacement of the sun east or west of the local meridian, morning negative, afternoon positive. The solar hour angle is equal to zero at solar noon and varies by 15 degrees per hour from solar noon. The sunset hour angle ω_s is the solar hour angle corresponding to the time when the sun sets and given by equation 3:

$$\omega_s = -\tan \psi \tan \delta \quad (3)$$

ψ represents the latitude of the site specified by the user.

7. Extraterrestrial radiation and clearness index

Solar radiation outside the earth's atmosphere is called extraterrestrial radiation. Daily extraterrestrial radiation on a horizontal surface, H_0 , can be computed for day n from the following equation:

$$H_0 = 86400 \frac{G_{sc}}{\pi} \left(1 + 0.33 \cos \left(2\pi \frac{n}{365} \right) \right) \quad (4)$$

$$(\cos \psi \cos \delta \sin \omega_s + \omega_s \sin \psi \sin \delta)$$

where G_{sc} is the solar constant equal to 1,367 W/m², and all other variables have the same meaning as explained in equation 1 and 2. Before reaching the surface of the earth, radiation from the sun is attenuated by the atmosphere and the clouds. The ratio of solar radiation at the surface of the earth to extraterrestrial radiation is called the clearness index, defined in equation 4:

$$\bar{K}_T = \frac{\bar{H}}{H_0} \quad (5)$$

where \bar{H} is the monthly average daily solar radiation on a horizontal surface and \bar{H}_0 is the monthly average extraterrestrial daily solar radiation on a horizontal surface. \bar{K}_T values depend on the location and the time of year considered; they are usually between 0.3 (for very overcast climates) and 0.8 (for very sunny locations).

8. Calculation of average efficiency

The array is characterized by its average efficiency, η_p , which is a function of average module temperature T_{a_c} :

$$\eta_p = \eta_r [1 - \beta_p (T_c - T_r)] \quad (6)$$

where η_r is the PV module efficiency at reference temperature T_r (25°C), and β_p is the temperature coefficient for module efficiency, T_c is related to the mean monthly ambient temperature T_a through Evans' formula (Evans, 1981) [10]:

$$[T_c - T_a] = (219 + 832 \bar{K}_t) \frac{NOCT - 20}{800} \quad (7)$$

where NOCT is the Nominal Operating Cell Temperature and \bar{K}_t the monthly clearness index. η_r , NOCT and β_p depend on the type of PV module considered. Such values can be manually entered into the model, but for "standard" technologies, assumed values are given in Table 1.

Table 1: PV module characteristics for standard technologies.

PV module type	η_r (%)	NOCT (°C)	β_p (%/°C)
Mono - Si	13.0	45	0.4
Poly - Si	11.0	45	0.4
a-Si	5.0	50	0.11
CdTe	7.0	46	0.24
CIS	7.5	47	0.46

The equation above is valid when the array's tilt is optimal (i.e. equal to the latitude minus the declination). If the angle differs from the optimum the right side of equation (8) has to be multiplied by a correction factor C_f defined by:

$$C_f = 1 - 1.17 \times 10^{-4} (s_m - s)^2 \quad (8)$$

where s_M is the optimum tilt angle and s is the actual tilt angle, both expressed in degrees.

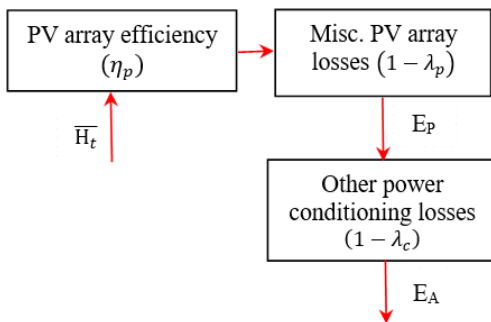


Figure 2: Flowchart for PV Array Model

9. Other corrections

The energy delivered by the PV array, E_p , is simply:

$$E_p = S \cdot \eta_p \cdot \bar{H}_t \quad (9)$$

where S is the area of the array. It has to be reduced by "miscellaneous PV array losses" λ_p and "other power conditioning losses" λ_c .

$$E_A = E_p (1 - \lambda_p) (1 - \lambda_c) \quad (10)$$

where E_A is the array energy available to the load and the battery. The overall array efficiency η_A is defined as:

$$\eta_A = \frac{E_A}{S \cdot \bar{H}_t} \quad (11)$$

10. Off-Grid Model

Off-grid renewable power can come from a variety of sources, ranging from large-isolated power grids to solar lights and solar home systems. In addition to households, off-grid renewables provide power for water pumping, street lighting,

telecommunications towers, rural schools and clinics, as well as for remote commercial and industrial facilities and other uses [11].

The off-grid model represents stand-alone systems with a battery backup, with or without an additional genset. The conceptual framework of the model is shown in Figure 3. Energy from the PV array is either used directly by the load or goes through the battery before being delivered to the load. The remainder of the load is provided by the genset if there is one, that is, stand-alone and hybrid systems differ only by the presence of a genset that supplies the part of the load not met directly or indirectly by photovoltaics.

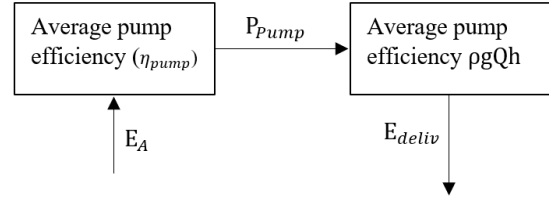


Figure 3: Energy transformation workflow.

The water pumping model is based on the simple equations found in Royer et al. (1998) [12] shown schematically in Figure 16. The daily hydraulic energy demand E_{hydr} , in J, corresponding to lifting water to a height h (m) with a daily volume Q (m³/d) is:

$$E_{hydr} = 86400 \rho g Q h (1 + \eta_f) \quad (12)$$

where g is the acceleration of gravity (9.81 m s⁻²), ρ the density of water (1000 kg/m³), and η_f is a factor accounting for friction losses in the piping. This hydraulic energy translates into an electrical energy requirement E_{pump} .

$$E_{pump} = \frac{E_{hydr}}{\eta_{pump}} \quad (13)$$

where η_{pump} is the pump system efficiency. If the pump is AC, this equation has to be modified to take into account the inverter efficiency η_{inv} :

$$E_{pump} = \frac{E_{hydr}}{\eta_{pump} \eta_{inv}} \quad (14)$$

Energy delivered is simply:

$$E_{deliv} = \eta_{pump} \min(E_{pump}, E_A) \quad (15)$$

where E_A is the energy available from the array (this quantity should be multiplied by η_{inv} in the case of an AC pump), and daily water delivered is obtained from:

$$Q_{deliv} = \frac{E_{deliv}}{86400 \rho g Q h (1 + \eta_f)} \quad (16)$$

Suggested array size is calculated simply by inverting the above equations and is therefore equal to E_{pump}/η_A where η_A is the overall array efficiency (see equation 10). This quantity is calculated on a monthly basis and the maximum over the season of use is the suggested array dimension. In the case of an AC pump, suggested inverter capacity is simply taken equal to the nominal array power. This is the only method possible since it is assumed that the pump power rating is not known (only the energy demand is known)

11. PVWP system in PVsyst environment

The selection of the PV must meet different criteria simultaneously:

- generate high quality electricity according to specific standards.
- withstand the high variability of solar radiation characteristics.
- require less maintenance interventions and costless.
- compete economically with other energy sources.
- fast and cost-effective compliance.
- Guarantee the water demand in time and reducing the unused energy level.

From the PVsyst database and technical information obtained from the manufacturer, comparisons were executed to determine the most efficient PV module among five alternative types taken in this study.

After creating the data file in the PVsyst for the selected area the first step is to define the orientation of the solar plane. The quick optimization of the solar energy should be accordingly with respect to function and aim of the proposed PV system. As our system will be used to provide water for irrigation purposes in summer period and for the fixed tilted plane type the maximums fall in the 23° tilted angle and azimuth 0°. For the summer period (April to September) the transposition factor resulted 1.06, loss in respect to optimum is -0.2% and global yield (in summer) on collector results 1307kWh/m² (see table nr 2).

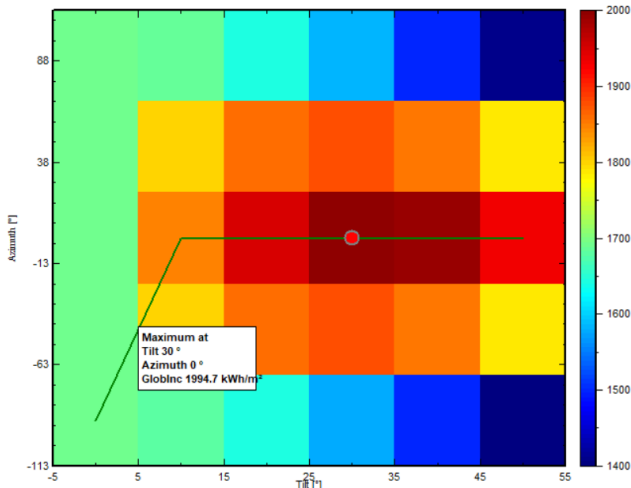


Figure 4: Optimization tilt and azimuth angle at the proposed PVWP system.

PVsyst enable the users to perform automatically a set of simulations, where one or more parameters are varied systematically according to a specified range. Optimization tools of the 'Orientation' suggest a tilt angle of 30° and azimuth 0°. In our calculation the tilt angle is suggested 23° up 30°. But in our case is approximated to 23° as the aim is to provide water during summer period global yield on collector is 1309 kWh/m² while for 30° is 1294kWh/m².

Table 2: The preliminary parameters chosen for the PVWP model.

Transposition factor	Loss in respect to optimum (%)	Global yield (in summer) on collector (kWh/m ²)
1.06	-0.2%	1307

In the second step it is obligatory to define the "Water needs" button selecting "Pumping Hydraulic Circuit" and one can choose among one of the three available systems (refer figure 4):

1. Pumping from a deep well, to a tank storage,
2. Pumping from a lake or river, to a tank storage,
3. Pumping into a pressurized tank, for water distribution.

In our case study pumping from a deep well to a tank storage is defined. The well can be 5 meters up to 15 meters deep. From the farmers statement, normally 10 meters deep well can guarantee the water demand referring the driest month (July) for more 10 hours for irrigation of carrots or potatoes. The actual well is around 15 meter and the water amount is able to provide 8 hours irrigation per day and the specific drawdown of -0.08m³/h with a maximum flowrate of 62.5m³/h, dynamic lower level -10m, the tank volume is defined 200m³ which can easily provide the water amount per each irrigation day with a reserve of 40%. Feeding altitude is selected 6.5m above ground level calculated as a result of the water parameters needed at the end of the circuit line.

Table 3: Main parameters from a deep well to a tank storage.

	Unit	Value
Static level	m	-5
Specific drawdown	m/m ³ h	-0.08
Maximum flowrate	m ³ /h	62.5
Lower dynamic level	m	-10
Hydraulic circuit	m	250
Number of elbows	pieces	30
Other friction losses	%	3-10
Tank volume	m ³	200
Tank diameter	m	6.5
Water full height	m	6.03
Feeding altitude	m	6.5
Pipe	"	4

The tank diameter volume is defined taking into account the daily water quantity demand referring the worst case (the most dry month of the year results July), crop type and soil type. The references for the water needs profile are provided form the literature given below in figure 5. Sprinkler irrigation systems are well adapted to carrot and potatoes irrigation. In the region, sprinkler designs of 12x12 m were common in carrot irrigation. Sprinkler flow rates varies from 0.3-4m³/h. Similar result, 2.57 m³/h sprinkler having flow rate at 2.38 atm pressure with 4.5/4.8 mm nozzle diameter was also mentioned elsewhere [13] in same region. Durations for using sprinklers with 0.3-1.0 m³/h and 1.5-2.5 m³/h flow rates were 9-10 h and 5-6 h. Yield or quality of carrot root is highly affected by carrot cultivar, fertilizer management, cultural practices in vegetation period and correct selection or management of irrigation system. In our study, carrot root yield was in the range between 60 and 85 m³/ha. Irrigation water was obtained from the ground water source in research region. Average electricity consumption for pumping unit volume of water and seasonal electricity consumption were determined as about 0.305 kwh/m³ and 5338 kwh/ha (17500x0.305), respectively. In research of, energy consumption of such pump was about 0.340 TL/kwh. It was calculated as 1815 TL/ha or \$485/ha. In generally water requirement for vegetable crop can be calculated by using the following formula [14]:

$$W_{req} = \frac{A * PE * P_c * K_C * w_a}{E_u} \quad a$$

Where: W_{req}=Peak water requirement (m³/day); A=crop area (20 000m²); PE =Pan Evaporation rate (mm/day) converted to m/day; (8-10 mm/day); P_c=Pan Coefficient (0.7 to 0.9); K_c=Crop Coefficient (0.8 to 1); w_a=wetted area (%) taken (90% for sprinkler irrigation); E_u=Emission uniformity of sprinkler irrigation (0.8).

By substituting the mentioned above values, the water requirement is approximately 137.7 m³/day

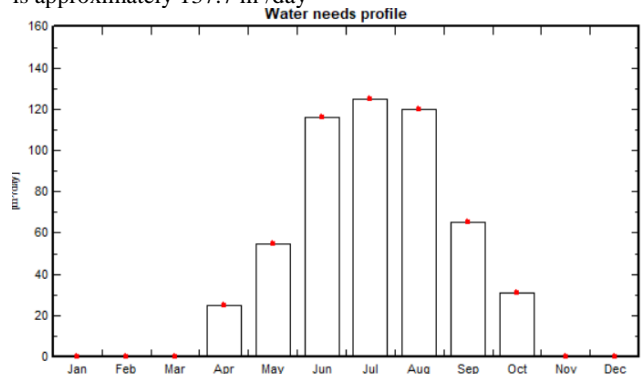


Figure 5: Water demand profile for the proposed case study.

As it can be seen from the water needs profile given in figure 5 the average yearly water demand is around 45 m³/d or 16 334 m³ for the whole year for the given surface in figure number 1.

The next step is select the most suitable water pump based on the water needs profile. This selection should take into the consideration the well type, control type and solar radiation potential as well. The simulation should be performed to provide the best solution in terms of specific energy, system and pump efficiency and reducing fraction of unused energy produced by the PV system. The result from the simulation carried out are summarized in table 4.

Table 4: Main technical parameters of the water pump

Centrifugal Multistage (Grundfos SOF 9-3 v30-300V)			
Maximal power	1400 W		
Voltage	170 V		
Max.Current	8.2 A		
Head min/Nom/Max (meterW)	5	15	25
Corresp.Flowrate	17	14.4	11.0
Corresp. Power	1400	1400	1400
Efficiency	16.6	41.9	53.7

Table 5: Main technical parameters of the PV module used in the study

	Technology	Specification
PV System	Generic/Si-poly	285Wp 30V
Sizing voltages		Vmpp (60°C) 31.2V Voc (-10°C) 49.9 V
Modules in series		3
	<i>Operating conditions</i>	
Vmpp	(60°C)	94V
Vmpp	(20°C)	111V
Voc		150 V
	<i>Plane irradiance 1000 kWh/m²</i>	
Impp		7.9A
Isc/Isc (STC)		8.4A/8.4A
Maximum operating power at 1000 W/m² and 50°C		0.8kW
Array nominal power (STC)		0.9kW

Inverter type for this case study is provided from the model universal controller 1000W and suggested control type MPPT - DC converter.

12. Results and analysis

From the simulation of the proposed PVWP system the final results for the efficiency of the system and other techno economic features.

In figure 6 it is given the flowrate as a function of available energy delivered at the pump. At the maximum head of 25m flowrate reaches the level of **11.0 m³/h**

The pump results DC motor and the maximum flowrate is 17 m³/h but in nominal condition the water flowrate then can be pumped is 14.4 m³/h. The water needs can be provided if the pump works 6-8 hour per day then 115m³/day can be discharged into the tank. That

is the water demand that system can be provided in one day referring the worst case (July period).

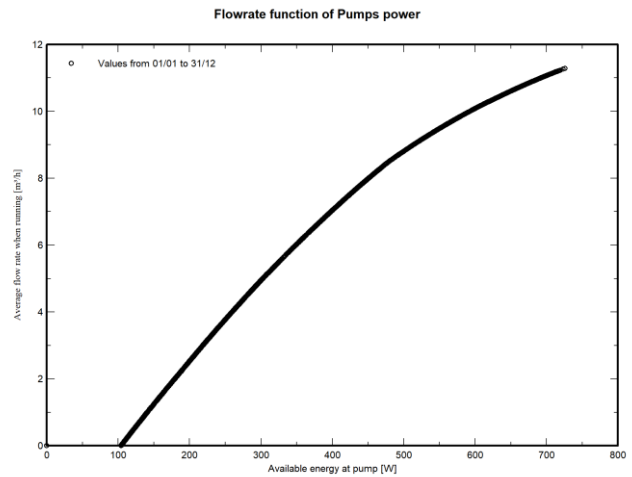


Figure 6: Flowrate function of pumps power.

Normalized productions (per installed kWp)

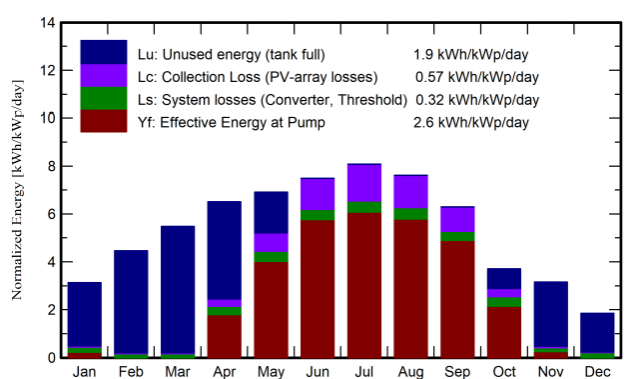


Figure 7: Normalized Energy (kWh/kWp/day).

In figure 7 the normalized production (kWh/kWp/day) per each month is given. The maximum production fall in July while in March the unused energy happen due to the zero water demand profile. In January up to May the fraction of unused energy prevails. In summer period from April to October the unused fraction becomes zero as the water demand is higher. The collection losses (PV-array losses) are higher during the summer period reaching the maximum value in July (0.57kWh/kWp/day). Converter losses are in the range of 0.32 (kWh/kWp/day).

Normalized Production and Loss Factors

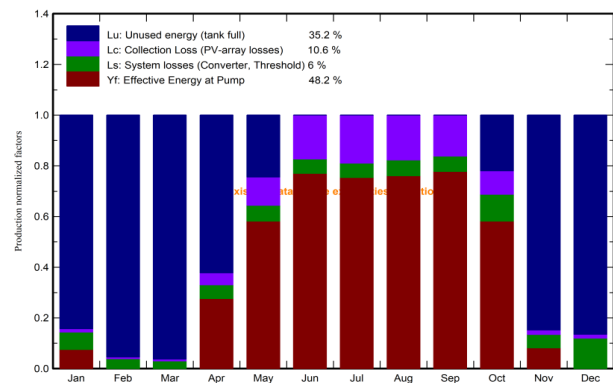


Figure 8: Normalized Production and Loss Factors.

In figure 8 the unused energy fraction results 35.2 % due to the water profile demand during winter season. PV array losses are 10.6% while effective Energy at pump results 48.2%.

Table 7: Main balances and results from the simulation of the selected PVWP system.

	GlobEff kWh/m ²	EarrMPP kWh	E_PmpOp kWh	ETKFull kWh	H_Pump meterW	WPumped m ³	W_Used m ³	W_Miss m ³	EArray kWh	PR ratio
January	94.0	76.6	6.3	61.0	11.43	100	0	0	76.6	0.076
February	121.5	97.1	0.0	88.3	0.00	0	0	0	97.0	1.000
March	164.9	128.9	0.0	118.5	0.00	0	0	0	128.9	1.000
April	190.1	144.6	46.1	85.8	11.52	741	750	0	144.5	0.276
May	209.2	156.1	106.6	36.4	11.81	1698	1705	0	156.0	0.582
June	219.2	159.0	148.0	0.0	11.63	2394	2571	909	158.9	0.710
July	244.1	173.5	161.4	0.0	11.67	2649	2657	1218	173.5	0.754
August	230.1	166.2	153.6	0.0	11.70	2537	2537	1183	165.9	0.761
September	184.0	135.4	125.7	0.0	11.63	2074	1931	19	135.4	0.778
October	111.7	86.2	57.2	17.8	11.47	907	961	0	86.1	0.582
November	91.8	73.2	6.6	58.8	11.64	111	0	0	73.1	0.082
December	55.5	45.0	0.0	36.7	0.00	0	0	0	44.9	1.000
Year	1916.2	1441.8	811.6	503.5	11.62	13211	13111	3330	1440.8	0.482

Legends

GlobEff Effective Global, corr. for IAM and shadings
 EarrMPP Array virtual energy at MPP
 E_PmpOp Pump operating energy
 ETKFull Unused energy (tank full)
 H_Pump Average total Head at pump

WPumped Water volume pumped
 W_Used Water drawn by the user
 W_Miss Missing water
 EArray Effective energy at the output of the array
 PR Performance Ratio

In table 7 Balances and main results per each month of the year are given. The water used throughout the year results 13111 m³ while the missing water results 3330 m³. Having in mind that system suggested to incorporate a water tank with 125 m³ which is taken 200 m³ providing a reserve of 30% more than the water needs. Other important outputs are carried out for evaluation in the case if the system changes (water pump or well type).

13. Conclusion

The present paper address various aspects related to PVWP energy systems for irrigation purposes in agriculture sector in Divjaka district. Nowadays, benefits coming from the PVWP system is becoming extremely beneficial from both technical and cost point of view and of course environmentally friendly. The perspective of a wide use of green power especially in agriculture sector motivates the policy makers in Albania to evaluate the possibility of funding the proposed systems.

The simulation from the study shows that for 2.0 ha, referring to the chosen PVWP system, the energy at pump becomes 812 kWh, specific energy 0.06kWh/m³, system efficiency 56.3%, pump efficiency 52.2% while the unused energy fraction results 34.9% (503kWh). The missing water rate is evaluated at a range of 19.6% which is covered by the extra dimension of the water tank.

The study shows very good results compared to the existing water pump systems (totally based on fossil or electricity from the grid) applied for irrigation purposes in Albania. Further investment in RES is essential for agri-food systems transformation and development, climate resilience and net-zero strategies by 2030 in Albanian context, as the majority of the rural population lies their economy on agriculture. The use of this kind of system could have an important contribution in the diversification of energy sources, mitigation of GHG, social and economic development of our country.

References

[1] Blankenship R, Tiede D, Barber J, W Brudvig G, Fleming G, Ghirardi M, Gunner M, Junge W, Kramer D, Melis A, Moore T, Moser C, G Nocera D, Nozik A, R Ort D,

Parson W, Prince R, Sayre R (2011) Comparing photosynthetic and photovoltaic efficiencies and recognizing the potential for improvement. Science (New York, NY) 332. <https://doi.org/10.1126/science.1200165>

[2] IRENA and FAO. 2021. Renewable energy for agri-food systems – Towards the Sustainable Development Goals and the Paris agreement. Abu Dhabi and Rome. <https://doi.org/10.4060/cb7433en>

[3] Elamri Y, Cheviron B, Lopez J-M, Dejean C, Belaud G (2018) Water budget and crop modelling for agrivoltaic systems: application to irrigated lettuces. Agric Water Manag 208:440–453. <https://doi.org/10.1016/j.agwat.2018.07.001>

[4] Hannah L, Roehrdanz PR, Ikegami M, Shepard AV, Shaw MR, Tabor G, Zhi L, Marquet PA, Hijmans RJ (2013) Climate change, wine, and conservation. Proc Natl Acad Sci U S A 110:6907–6912. <https://doi.org/10.1073/pnas.1210127110>

[5] IRENA and FAO. 2021. Renewable energy for agri-food systems – Towards the Sustainable Development Goals and the Paris agreement. Abu Dhabi and Rome. <https://doi.org/10.4060/cb7433en>

[6] Renewable, International, and Energy Agency. 2020. Renewable Energy and Jobs – Annual Review 2020

[7] Malka, L., Konomi, I., Alcani, M., Gjeta, A., & Bebi, E. (2020). Off-grid hybrid PV plants used to supply autonomuos internet base stations supporting the mitigation of GHG in Albania Case study: Bulqiza district, Albania. 178(4), 174–178. <https://stumejournals.com/journals/ia/2020/4/174>

[8] Duffi e, J.A. and Beckman, W.A., Solar Engineering of Thermal Processes, 2nd Edition, John Wiley & Sons, 1991.

[9] Evans, D.L., Simplifi ed Method for Predicting Photovoltaic Array Output, Solar Energy 27,6, 555-560, 1981

[10] IRENA (2018), Measurement and estimation of off-grid solar, hydro and biogas energy, International Renewable Energy Agency (IRENA), Abu Dhabi

[11] Royer, J., Djiako, T., Schiller, E. and Sy, B.S., Le pompage photovoltaïque: manuel de cours à l'intention des ingénieurs et des techniciens, Institut de l'Énergie des Pays ayant en commun l'usage du Français, 56, rue Saint-Pierre, 3e étage, Québec, QC, Canada, G1K 4A1, 1998

[12] D. Yavuz "The Energy Requirement of Sprinkler Irrigation". Master's Thesis. Selçuk University, Graduate School of Natural and Applied Sciences, Department of Agricultural Structures and Irrigation. 2006, 49 ps (In Turkish)

[13] Hossain, I. (2018). EFFECTIVE PUMPING SYSTEM USING PVSYST TO HARNESS SOLAR POWER FOR. 3(3), 47–55. <https://doi.org/10.22271/chemi.2020.v8.i6q.10928>

Study of the magnetic field of a magnetic treatment device for agricultural materials

Nedyalko Nedyalkov, Miho Mihov, Viktoriya Kancheva - Institute of Soil Science, AgroTechnology and Plant Protection "Nikola Pushkarov", Sofia, Bulgaria

SUMMARY: *The type of supply voltage of the coil to achieve maximum induction and uniformity of the magnetic field in the magnetic chamber, where the processed material is determinate. The experimentally obtained dependence curves $B = f(U)$ can be used to optimize the regime parameters when processing various agricultural materials in a magnetic field.*

KEYWORDS: MAGNETIC TREATMENT, MAGNETIC INDUCTION, MAGNETIC FIELD, SEEDS, PLANTS

Biophysical methods for stimulating seeds and plants increase their energy balance through the internal transformation of energy (regardless of its origin) into electrical, and hence the electrical potential of the cell membrane. As a result, metabolism and growth (maturation) increases, which leads to increased yields. [4.5.]

The effect of electromagnetic fields on seeds has a biological stimulation of plants. The results of the experiments show that it is possible to increase the yield of cereals by up to 20%, increase the root mass of sugar beet by an average of 39% and its leaf mass by up to 25% by stimulation in a magnetic field. Impact with electromagnetic fields of different intensities in macro experiments with potatoes has led to an increase in yield by an average of about 23.2%, germination energy of seeds is preserved longer, plants grow faster and show higher resistance to disease, accelerating maturation, preserving the quality of products for a long-time during storage, etc. [1.3.]

OBJECT AND PURPOSE OF THE RESEARCH

A device for processing agricultural products with a magnetic field has been developed, Fig.1. The device works as follows. The material to be processed is placed in the magnetic

chamber located on the lower pole piece. A stirring mechanism is driven by a gear motor, which mixes the processed material. The exposure time is determined by the type of material being processed. Simultaneously with starting the engine, the coil, which creates the magnetic field, is powered. A magnetic field with a certain value of magnetic induction is created in the air gap in which the magnetic chamber with the processed material is located. After the set processing time has elapsed, the motor and coil supply are switched off. The container is emptied and refilled with raw material. In [2] were identified some of the main design parameters of the device, in terms of the type of magnetic chamber, the drive and the type of the stirring mechanism to create homogeneity of the material during processing. When exposed to a magnetic field on agricultural products are affected not only the design parameters of the device, but also the mode parameters of processing: value of magnetic induction, exposure, type and distribution of the magnetic field.

The aim of the present study is to establish the dependence of the magnetic induction on the values and type of supply voltage of the coil, as well as the distribution of the magnetic field in the area of the processed material.

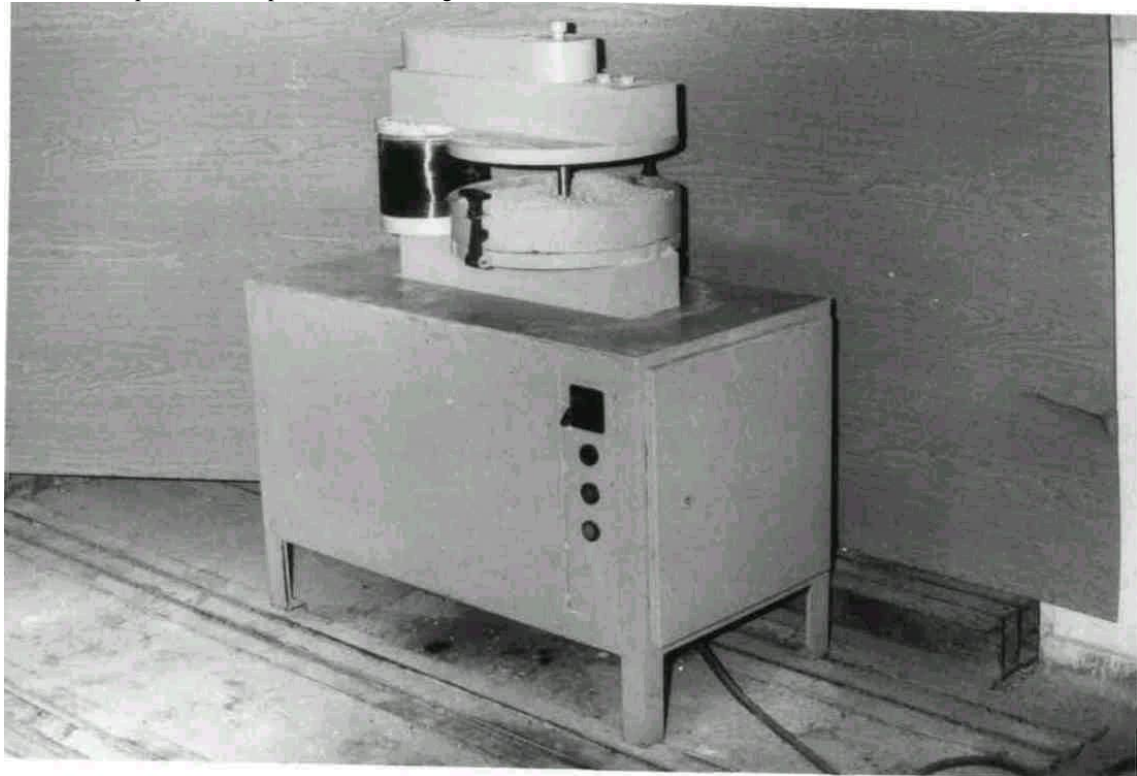


Fig. 1. Device for processing agricultural materials with magnetic field

METHODS AND MEANS

To establish the dependence of the magnetic induction on the type and values of the supply voltage of the coil, experimental studies were performed in which the coil was supplied with alternating sinusoidal voltage 0-250 V, 50 Hz with a variation step of 10 V; constant voltage - 12 V; 24 V; 36 V and 48 V, single-phase one-and-a-half-cycle circuit; DC voltage, single-phase bridge circuit "Gretz". The supply voltage in the last two variants is changed from

0-250 V in steps of 10 V. The voltage is regulated by means of an autotransformer. The measurement of the magnetic induction takes place at a pre-selected point on the lower pole piece, where the processed material is placed.

To determine the distribution of the magnetic field, the induction of the magnetic field on the lower pole piece, which has a diameter of 400 mm, was measured. The measurement of the magnetic induction starts from the centre of the nozzle (radius $R = 0$) at equal distances in two diametrical directions, located at 90

degrees to each other up to a radius of $R = 200$ mm. The measurement was performed with a teslameter.

RESULTS OF THE SURVEY

When supplying the coil with DC voltage (0-250V, 50 Hz) the measured magnetic induction in the area of the lower pole piece is very small $1.10 \cdot 10^{-5}$ - $5.10 \cdot 10^{-5}$ T. This is due to the large distance between the two pole tips $h = 0-70$ mm. At $h = 0$ the measured induction is $B = 1.10 \cdot 10^{-3}$ T. As the height h increases, the magnetic induction B decreases at $h = 70$ mm - the induction is $B = 1.10 \cdot 10^{-4}$ T. In the existing design of the magnetic system, the distance between the pole pieces is fixed by the geometric dimensions of the coil, $h = 200$ mm. At a later stage of device improvement, this distance can be optimized.

Four 12 V rechargeable batteries were used to supply the coil with constant voltage, through the series connection of which voltages of 12 V, 24 V, 36 V and 48 V were obtained. The

measured magnetic induction was 0.03T, 0.047T, 0.062T and 0.076T, respectively. The application of this type of power supply, in the study, is hampered by the possibility of using a source of constant voltage up to 250 V.

The obtained results from the measurement of the magnetic induction when supplying the coil with direct voltage, single-phase one-half-cycle circuit and supply with direct voltage, single-phase bridge circuit are processed and based on them the dependence curves of magnetic induction $B = f(U)$ are constructed. The curves are shown in Fig.2. From the type of curves obtained, it can be found that the values of magnetic field induction when fed with a one-and-a-half-cycle rectification circuit are significantly lower than when the coil is supplied with a bridge rectification circuit. In the electrical circuit of the developed device for magnetic processing the coil will be supplied by a bridge circuit "Gretz" for voltage rectification.

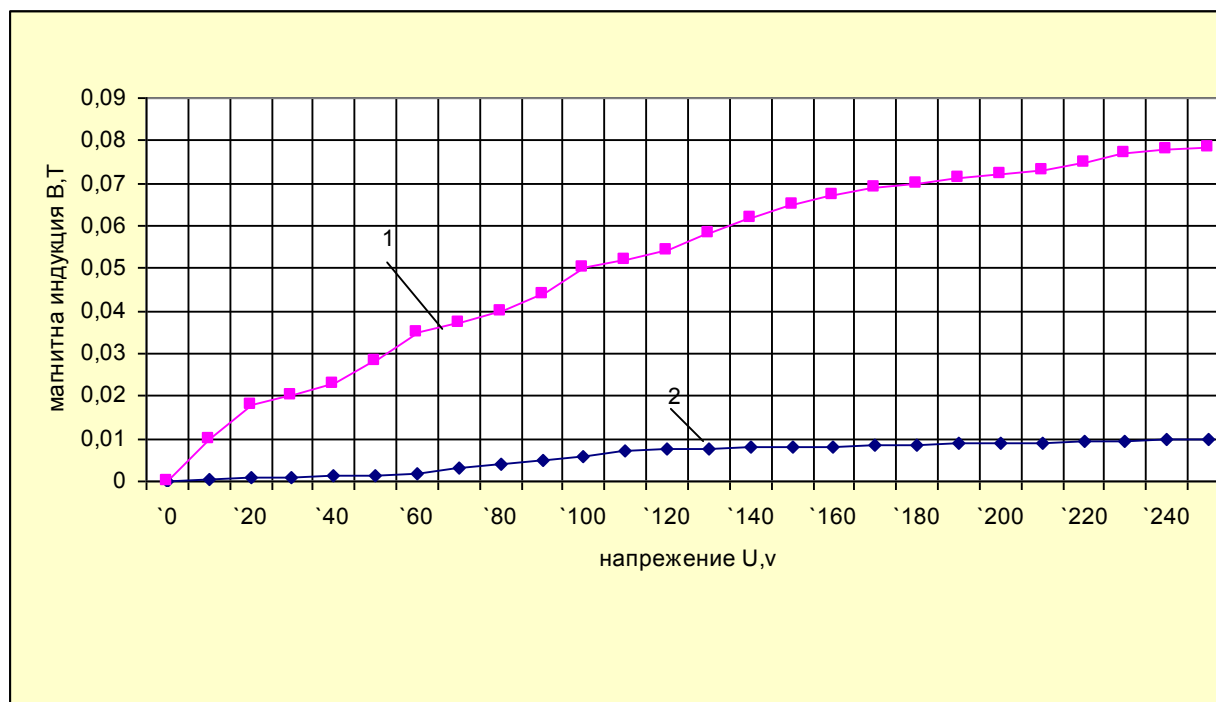


Fig. 2. Dependence of the induction of the magnetic field B on the supply voltage of the coil U : 1 - single-phase bridge circuit; 2 - single-phase one-and-a-half-cycle circuit

The recommended values of magnetic induction in pre-sowing treatment of seeds from different crops, as well as other agricultural materials are unknown., whether have been determined experimentally or analytically by "Gretz".

When processing agricultural materials with magnetic field, using the obtained dependence curve $B = f(U)$, it will be possible to realize variants with different magnetic induction of the field between the two pole tips of the magnetic system of the device. This will allow to optimize the regime parameters when processing different agricultural materials with magnetic field.

When studying the distribution of the magnetic field in the area of the processed material, the coil is supplied with a direct

voltage of 220 V by means of a bridge circuit "Gretz". The measured values of the magnetic induction B , according to the procedure described above, in six radial directions, located at 60 degrees to each other, are the same - $B = 0.075$ T.

The following experiment was performed to illustrate the distribution of the magnetic field. An even layer of ferromagnetic powder is placed on the lower pole piece, where the processed material is placed, fig.3. After switching on the magnetic processing device, the ferromagnetic powder is magnetized in the direction of the magnetic field lines, Fig.4. The relatively uniform distribution of ferromagnetic particles in the magnetic field between the two pole pieces can be seen.



Fig. 3 Ferromagnetic powder before treatment with magnetic field



Fig. 4. Ferromagnetic powder after treatment with magnetic field

Based on the results obtained from the measurement of the magnetic induction and the magnetization of the ferromagnetic dust, it can be assumed that a relatively uniform distribution of the magnetic field is created in the material processing area, i.e., the material is processed evenly in its full volume, according to the set exposure.

CONCLUSIONS

It was found that a relatively uniform magnetic field is created in the material processing area.

The values of the magnetic induction of the field when supplying the coil with a one-and-a-half-cycle voltage rectification circuit are much lower than when supplying with a bridge rectification circuit "Gretz".

When processing agricultural materials with magnetic field, using the obtained dependence curve $B = f(U)$, variants with different magnetic induction of the field between the two pole tips of the magnetic system can be realized, which will allow to optimize the processing parameters. of various agricultural materials in a magnetic field.

LITERATURE

1. Dohorov, P.G., 1984. Prospects for the use of electromagnetic fields in grain production. "Вопросът Бионики", Научните трудове, т.3-14, Алма-Ата. (RU)
2. Nedyalkov, N.A., 2010. Study to establish some basic parameters of the device for magnetic seed treatment. Agricultural machinery, issue 3, p 21-23. (BG)
3. Govedarica, M., Milosevic, N., 2012. Effect of electromagnetic stimulation on soil microbial activity. Biophysics in agriculture production, University of Novi Sad, Tampograf.
4. Marinkovic, B., Ilin, Z., Marinkovic, J., Culibrk, M., Jacimovic, G., 2012. Potato yield in function variable electromagnetic field. Biophysics in agriculture production, University of Novi Sad, Tampograf.
5. Takac, A., Gvozenovic, G., Marinkovic, B., 2012. Effect of resonant impulse electromagnetic stimulation on yield of tomato and pepper. Biophysics in agriculture production, University of Novi Sad, Tampograf.

An overview of agriculture sector in terms of fuel type and systems used for irrigation purposes.

Case study: Divjaka region, Albania

^aIlirian Konomi, ^bElena Bebi, ^cLorenc Malka, ^aErmonela Rrapaj

^aDepartment of Hydraulics & Hydrotechnics, Faculty of Civil Engineering, Polytechnic University of Tirana, Albania

^bDepartment of Production and Management, Faculty of Mechanical Engineering, Polytechnic University of Tirana, Albania

^cDepartment of Energy, Faculty of Mechanical Engineering, Polytechnic University of Tirana, Albania

ikonomi64@gmail.com, lmalka@fim.edu.al

Abstract: *In locations where electricity is not available and distribution lines are far away from the connection point, than other means are necessary to provide water for different applications especially in agriculture sector. Using a diesel pump to deliver water account economic and environmental problems. Fuel prices affect the overall costs of diesel-powered water pumping system thereby reducing the incomes from the sale of vegetables or other planted crops. In addition, the use of a diesel-powered water pump system can lead to considerable amount of CO₂ released to the surrounding which cause global warming. A possible solution to these problems is using renewable energy source like solar power, which is environmentally friendly and available for free. This paper focus on the identification of sector energy consumption and the possibility of application of PVWP system in the agriculture sector. Several economic analyses have been conducted to establish the best cost-effective solution for irrigation in agriculture sector. The possible benefits generated by the PVWP system implementation for the selected region should be highlighted, as well as the effects of the most sensitive parameters. The solar potential in the site showed that PVWP can be the best solution to provide water for irrigation compared to other traditional water pumping technologies and also can reduce the dependency from fossil fuel powered water pumps and can help the diversification of the agriculture sector especially.*

Keywords: PV-PUMP STATION, CO₂, GHG, RETScreen Expert.

1. Introduction

Public interest in the issue of irrigation water pricing has increased worldwide in recent years, with increasing awareness of water scarcity and greater appreciation of the opportunity costs of allocating water among competing uses. Many of the world's large-scale irrigation projects were constructed and placed in service in an era when water was relatively abundant or when the cost of developing water supplies in arid regions seemed a reasonable expense for expanding agricultural production and generating economic growth. Over the years, the incremental costs and benefits of irrigation have changed, as have public preferences regarding the allocation of water among agricultural, municipal, and environmental uses. The use of PVWP technology for irrigation is considered an innovative and sustainable solution with the aim to provide cost-effective solution within off grid PV concept. Such systems can promote the use of agriculture land, especially in remote areas of Albania. The combination of PVWP technology with water saving irrigation techniques and sustainable management of the groundwater resources can lead to several benefits. The integration of distributed renewable energy in agriculture sector can bring a lot of economic benefits to the farmers including the reduction of specific energy use and also can help to the mitigation of GHG emissions. From the technical point of view this system can offer the improvement of grid reliability and limitation of power outages, protection of critical loads, independence from national grid supply, and increased energy security coupled with a fixed energy cost which is immune to future tariffs and fossil fuel costs increases. This article presents a real application "Photo Voltaic Water Pump" (PVWP) installed in Divjake.

After II WW following the increase in agricultural potential, the region gained significant importance in the economy of the country. This paper assesses the possibility of installing PVWP system at site including an existing greenhouse. The RETScreen software and PVsyst is used for the feasibility and financial viability evaluation. The study found out that the Divjaka municipality part of the Fier county has the highest solar irradiation in Albania, recorded 4.56 kWh/m²/day. The financial indicators like the internal rate return (IRR), equity payback years, cumulative cash flows and simple profitability index all indicated that the agriculture sector is the best option for the development of

solar energy. The impact of the development of these plants will also have a considerable impact on the environment since the research on the field shows a great potential in the reduction in the emission of greenhouse gases (GHG), in some cases around 93%. Such systems are foreseen to play a key role in a stable, costless and emission-less way especially in off-grid concept applications. The performance, availability, costs and carbon intensity of photovoltaic power all indicate that this technology can make a very substantial contribution to reduce carbon emissions and gain carbon credits.

Similarly, in the study of [1] it is shown that Off-grid PV concept applied in telecommunication sector can bring a lot of benefits, especially in the very remote areas. Hence, PVWP systems can be used in the agriculture sector for irrigation purposes.

In the other hand the depletion of fossil fuel and the negative effect on the environment as well as the potential techno-economic merits of "hybrid combinations" identified as a good solution moving towards reliable and more feasible energy systems based on renewables [2]. As the need for clean, sustainable energy increases, and renewable technologies get ever more advanced, more projects had been developed in greater sizes and complexities, including on-grid and off-grid solutions based on RES.

Today, PV is one of the fastest-growing renewable energy technologies and is ready to play a major role in the future global electricity generation mix and a contribution for some 3.8 million jobs, or nearly a third of the sector total [3].

Using solar PV to power mini-grids is an excellent way to bring electricity access to people who do not live near power transmission lines, particularly in developing countries with excellent solar energy resources and reducing the negative effect on environmental.

The cost of manufacturing solar panels has plummeted dramatically in the last decade, making them not only affordable but often the cheapest form to be replaced and integrated in existing power systems. Solar panels have a lifespan of roughly 30 years and come in variety depending on the type of material used in manufacturing.

2. Site background and installation of proposed PV-Water pump station

In our case study the installation place will be located in Divjaka (41°02'158"N and 19°53'26"E) as it is shown in figure 1. The area has an altitude of 90 m above sea level and the measured average

annual air temperature results 15.24°C. Atmospheric mean pressure value and wind velocity measured at 10m altitude results 97.38kPa and 1.1 ms⁻¹.



Figure 1: The property of the proposed PVWP location

The property area chosen for this case study is around 2.0 ha and has an existing water well of 15 m deep (circle in blue). Thanks to the water sources available, the water quantity is provided from the well is enough to irrigate that surface for 8-10 hours per day with no missing water identified.

The property has a modern greenhouse with net surface of 0.5 ha usually used for different crops such as potatoes, tomatoes, and carrots. Daily water amount for irrigation depends on weather condition and temperature. The mean earth temperature varies from 5.6°C in January up to 25.26°C in August while precipitation varies from 25.73mm in July up to 118.5mm in November.

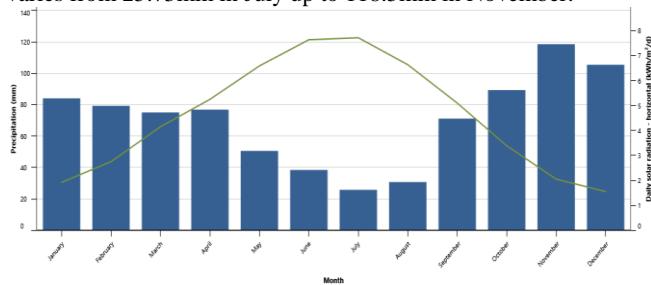


Figure 2: The proposed PVWP location daily solar radiation kWh/m²/day.

Actually, the owner of the farm uses two different pumps supplied from two different energy sources: Electricity and diesel pump. The technical parameters and the specific consumption are provided from the owner’s monthly bill.

From the model and data provided from Albanian Meteorological Institute it is shown that this region has a high solar potential.

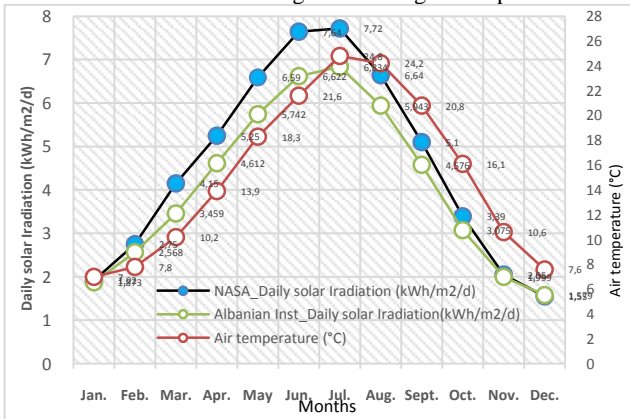


Figure 3: Daily solar radiation kWh/m²/day at the proposed location.

The main two problems discussed are: the connection point with the national electricity distribution grid and the process towards a cleaner and safer environment as the main fuel type (73%) is

provided from fossil powered water pumps is considered in this work. From [4] and its Earth Science research program has long supported satellite systems providing important weather data capable to be fully integrated in RETScreen model. These data include long-term climatologically averaged estimates of meteorological quantities and surface solar energy fluxes. These satellite and model-based products have been shown to be accurate enough to provide reliable solar and meteorological resource data over regions where surface measurements are sparse or non-existent. The highest values are observed during the summer season of the year, while the lowest values are observed in the winter months. The highest solar radiation value 6.834 kWh/m²/d is reached in July, while the lowest value 1.55 kWh/m²/d hits in December. According to Albanian Institute of Geo-Sciences, Energy, Water and Environment the annual mean solar radiation and temperature for Divjaka region is 4.082 while referring to NASA and 4.56 kWh/m²/d (11% lower).

Table 1: The site-specific solar energy data. Divjaka region. [Solar database and PV software©2022 Solargis]

Specific photovoltaic power output	PV _{OUT} specific	1554.8 kWh/kWp	
Direct normal irradiation	DNI	1725.2 kWh/m ²	
Global horizontal irradiation	GHI	1640.9 kWh/m ²	
Diffuse horizontal irradiation	DIF	620 kWh/m ²	
Global tilted irradiation at optimum angle	GTI	1912.5 kWh/m ²	
Optimum tilt of PV modules	OPTA	34/180 °	
Air temperature	TEMP	17.4 °C	
Terrain Elevation	ELE	80 m	

From Global Solar Atlas, energy planners can generate suitable site information for preliminary studies in EU-28 countries as they consider default values for many factors that are important for a design of a photovoltaic system. For more professional and detailed estimation it is used PVsyst tool that allow configuration of the proposed projects using more detailed solar and weather data as primary inputs to the simulation.

3. An overview of the Albanian Energy system.
3.1 Agriculture sector

Under the pressure of an increased awareness related to environmental issues and costs from the existing energy system in Albania, technological progress and the liberalization of the energy market, in the last 15 years lead to development of wind and solar exploitation technologies in Albania [5]. Renewable energy sources, including solar, wind, hydro, biofuels and other future renewable sources are at the centre of the transition towards a less carbon-intensive and more sustainable energy system. [6].

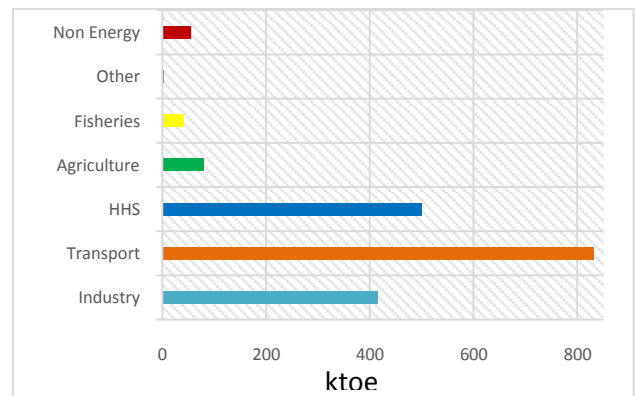


Figure 4: Final Energy Consumption by Sectors (ktoe) in Albania

2018 [5].

As it can be seen in figure 4 the final energy consumption in agriculture sector is around 80.32 ktoe. Transport sector and household are the main two sectors accounting 64% of the total final energy consumption in the country.

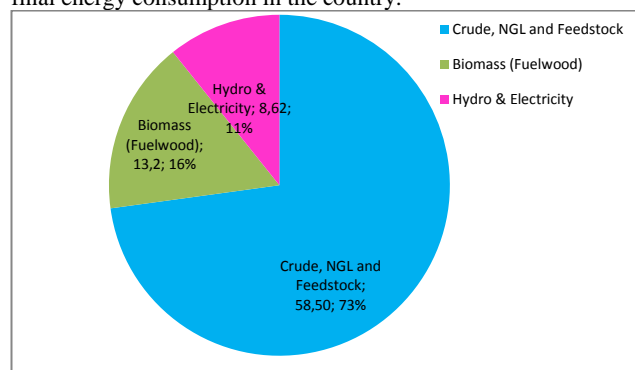


Figure 5: Agriculture Energy Consumption by fuel type, 2018. [5]

In figure 5 the consumption by fuel type in agriculture sector is given. The fossil fuel type account for 73% of the final energy consumption in agriculture sector, while electricity and biomass occupy the rest. The reduction of fossil fuel and electricity consumption within agriculture sector is the main focus of this research work.

4. Renewable energy strategy and progress

4.1 Solar energy

The Paris Agreement sets a goal to limit the increase in global average temperature to well below 2°C above pre-industrial levels and to attempt to limit the increase to 1.5°C. Implicit in these goals is the need for a transition to a low-carbon energy sector, which accounts for two-thirds of global emissions. RES, coupled with energy efficiency gains, can provide 90% of the CO₂ emissions reductions in the roadmap to 2050. Renewable energy is therefore a key component of Nationally Determined Contributions (NDCs)—the central implementation tool for countries under the Paris Agreement. At present, the level of detail contained in NDCs differs from country to country, with little in-depth analysis and limited quantitative information about the role of renewable energy in meeting greenhouse gas (GHG) emission reduction targets [7]. Based on the targets projected in global level Albania is making efforts to reduce the rate of electricity import and improve its security of supply fully in line with “Paris Agreement” requirements. The Albanian ministry of Energy and Transportation and its dependency institutions has compiled the *"The National Energy Strategy 2018-2030"*, consisting on 6 possible scenarios of energy's transition process toward a sustainable and reliable energy by shifting Albania to decentralized renewable energy market, and energy efficiency. This strategy requires reaching a RES share of 42% to the total energy consumption and also reducing CO₂ (referring 2016) level up to 11.5% by the end of 2030. The first goal can be achieved by large scale integration of RES capacities, especially wind generation capacities [8]. The second national energy goal, compared to the baseline scenario in 2016, should be also fully in line with EU objectives, its commitment is to reach a reduction of 11.5% of CO₂ emissions by the end of 2030. The RES share in global electricity generation reached almost 27% in 2019, renewable power as a whole still needs to expand significantly to meet the SDS share of almost half of generation by 2030 which requires the rate of annual capacity additions to accelerate the process [9].

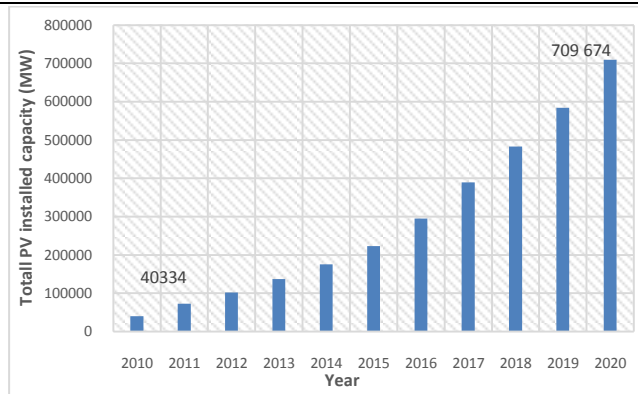


Figure 6: The global installed capacity trends of the PV systems.

In the graph in figure 6 the global installed PV capacity is given. The growth of PV capacity worldwide tends an exponential progress and results 18 times more in 2020 compared to 2010.

Considerable interest in RES and significant increases in cost of imported oil and very frequent services of related power generation technologies have compelled various countries to search for low-cost energy sources and improved technologies based on RES, PV and synergies between systems to achieve lower cost of electricity generation. Also, limiting the global average temperature rise to 1.5°C will require all sectors of the economy with increasing need for energy to reach zero carbon dioxide (CO₂) emissions early in the second half of this century. Photovoltaics (PV) is a key technology option for realising a decarbonised power sector and sustainable energy supply [10]. Most of those options rely on renewable necessarily supported from energy storage systems (ESS) [11].

5. Off – Grid PV systems applications

Off grid PVWP systems applications have been studied to cover a lot of issues, especially to provide water for drinking purposes in the areas that suffer the lack of electricity. Nevertheless, the drastic fall in prices of PV modules due to the new-born production and costless technologies of the PV lead to increased interest on research and development of off grid PV systems, encouraging greater system flexibility and large-scale integration. The research is mainly focused on system design, optimization of system components (such as BOS and solar array performance), and technical and economic comparisons between PV and other traditional stand-alone fossil powered sources. There is a lack of compatibility or similarity between two or more facts including the systematic optimization of energy systems, having in mind the irrigation water requirement (IWR), water resource availability, and crop yield under different water supply conditions. System failures and corresponding economic losses still occur due to the inadequacy of system integration with the environment. In most works done so far, PVWP systems have been considered as independent electricity stations without taking into consideration how the system is affected by the environment (e.g., IWR and water resources). Thus, the first two research questions are: how does the variation in Irrigation Water Requirement (IWR) during the irrigation season affect PVWP systems design and effectiveness (used and unused solar fraction)? and how can the proposed PVWP systems be optimized from an integrated system perspective (taking into consideration water resources in the site)? It is also essential to identify the technical, economic and environmental constraints that can affect the 3 different types of PVWP systems.

1. Deep well to storage.
2. Lake or River to storage.
3. Pressurization

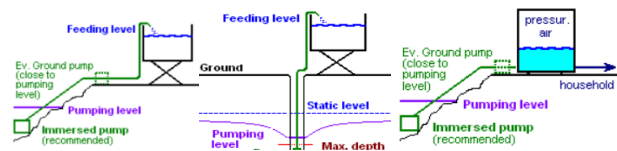


Figure 7: (a) deep well to storage; (b) Lake or River to storage and (c) Pressurization (source PVSyst)

Such systems can be applied using open or under pressure water tank. The pump can be immersed or can be positioning on the ground level involving in some cases the need for a boost pump.

6. Economic aspects of PV systems

Three key factors are essential when designing wind power plants. First there must be a sufficient source of solar potential in the proposed region, the PV technology must be promising as well as cost effective. Studies has shown that it is cost-effective for small loads (<10 kWp) need lower capital costs than grid extension and have lower O&M costs than gensets and primary batteries [12]. This section deals with the economic aspects of building a PVWP system with daily water consumption.

Any factor that leads to lower total lifecycle costs, or that yields greater kWh over the chosen analysis period, lowers the LCOE of a PV system. The total lifecycle cost in the numerator is a function of the initial capital cost (which primarily includes the module, the installation hardware and labour, and transaction costs for system installers and financiers), as well as ongoing operation and maintenance expenses (which oftentimes includes inverter replacement) and decommissioning costs including module collection and recycling. The total lifecycle energy production (the kWh in the denominator) is a function of location as well as module and system reliability and performance [12].

The global weighted-average LCOE of utility-scale PV plants declined by 82% between 2010 and 2019, from around \$0.378/kWh to \$0.068/kWh in 2019, with a 13% reduction year-on-year in 2019. At an individual country level, the weighted average LCOE of utility-scale solar PV declined by between 66% and 85% between 2010 and 2019.

7. PV Project Costs

Although the cost of PV panels energy has dropped dramatically in the last 10 years, technology requires a higher initial investment than traditional fossil fuel generators. Approximately 55% of the cost goes to module, 15% to inverter and the rest is belongs to BoS and installation costs (see graph in figure 8).

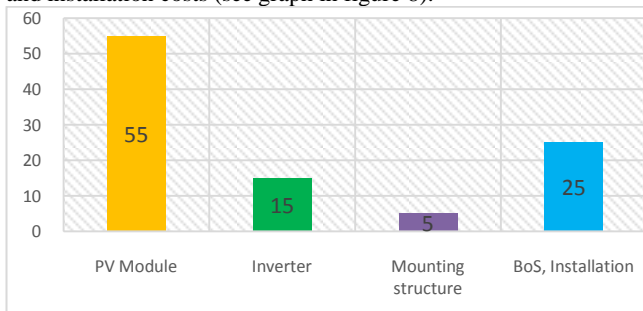


Figure 8: Cost breakdown of PV system components (%) [1]

8. Capital Investment Cost

With very rapid reductions in solar PV module and balance of system costs, utility-scale solar PV is now increasingly competing head-to-head with alternatives and without financial support. Lower solar PV module prices and ongoing reductions in balance of system costs remain the main driver of reductions in the cost of electricity from solar PV. The costs for renewable energy technologies reached new lows again last year. Solar and wind power have emerged as the most affordable power source for many locations and markets, with cost reductions set to continue into the

next decade. The latest improved manufacturing processes and enhanced module efficiency enabled are the key drivers of lower module costs. In addition, as project developers gain more experience and supply chain structures continue to develop in more and more markets, declining BoS costs have followed. This has led to an increased number of markets where PV systems are achieving competitive cost structures and resulted in falling global weighted-average total installed costs [1]. In 2019, significant total installed cost reductions have occurred across all the major markets such as China, India, Japan, Republic of Korea and the United States. An increasing number of cost competitive projects in India led to weighted average total installed costs of \$618/kW in 2019, around a fifth lower than in China. However, competitive costs structures are not confined to established markets anymore. Between 2010 and 2019, total installed costs have declined between 74% and 88% in markets where historical data is available back to 2010. The global capacity weighted-average total installed cost of projects commissioned in 2019 was \$995/kW, 18% lower than in 2018 and 79% lower than in 2010 (see graph in figure 6). Based on the costs of the developed projects around the globe, yearly variation of total installation cost and LCOE is given graphically in figure 9.

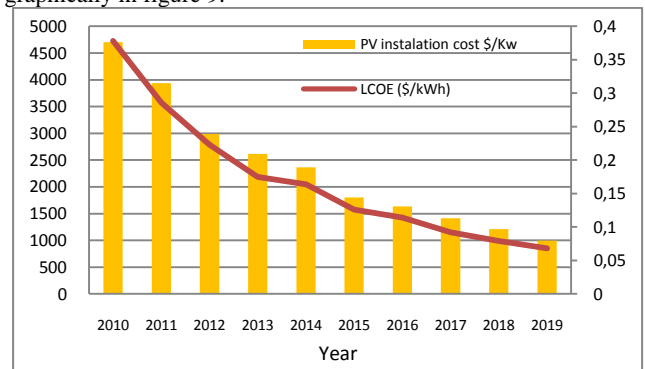


Figure 9: Global weighted average total installed costs, capacity factors and LCOE for PV, 2010–2019 [1-3]

An important driver of improved competitiveness historically, the downward trend in solar PV module costs continued during 2019. By the end of 2009 and 2019, crystalline silicon module prices declined between 87% and 92% for modules sold in Europe, depending on the type. The weighted average cost reduction could be in the order of 90% during that period. More recently the cost of mainstream module technology declined 14% between December 2018 and December 2019, reaching \$ 0.27/W. A wide range of costs exists, however, depending on the type of module considered, with costs for December 2019 varying from as low as \$0.21/W for the lower cost modules to as high as \$0.38/W for all black modules. The cost of high efficiency crystalline modules at \$0.37/W was slightly above thin film offerings, which sold for \$0.36/W during that period. These costs declines and the advances in the ability to securely operate the grid with high shares of variable renewables are not only decarbonizing the electricity sector but are unlocking low-cost decarbonization in the end-use sectors in conjunction with increased electrification. On average, in 2019, balance of system costs (excluding the module and inverter) made up about 64% of total installed costs. In 2019, total BoS costs ranged from a low of 48% in India to a high of 76% in the Russian territories. Overall, soft cost categories for the evaluated countries made up around 40% of total BoS costs and about a quarter, on average, of the total installed costs. In 2016, these values were a third and 17% respectively.

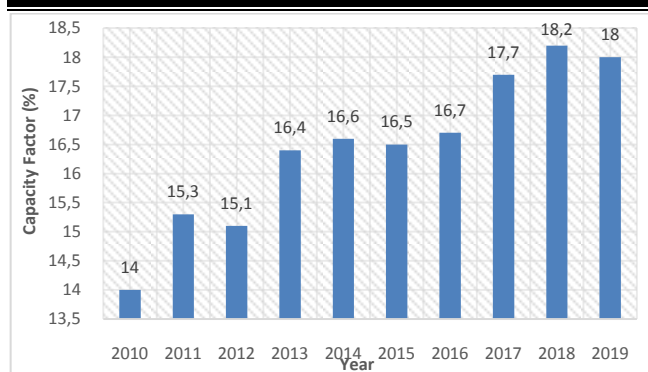


Figure 10: Global weighted average capacity factors for utility-scale PV systems by year of commissioning, 2010–2019

The global weighted-average capacity factor for new, utility-scale solar PV, increased from 13.8% in 2010 to 18.0% in 2019. This was predominantly driven by the increased share of deployment in sunnier locations. A constant increased between 2010 and 2018 of the capacity factor is given in Figure 7 [11]. The development of the global weighted-average capacity factor is a result of multiple elements working at the same time. Higher capacity factors in recent years have been driven by the shift in deployment to regions with higher irradiation, the increased use of tracking devices in the utility-scale segment in large markets and a range of other factors that have made a smaller contribution (e.g., reduction in system losses).

9. Operation and Maintenance Costs

The Operation and Maintenance costs of utility-scale solar PV plants have declined in recent years. However, in certain markets, the share of O&M costs in total LCOE has risen, as capital costs have fallen faster than O&M costs. O&M cost declines have been driven by module efficiency improvements leading to reduced surface area required per MW of capacity. At the same time, competitive pressures and improvements in the reliability of the technology have resulted in system designs optimised to reduce O&M costs and improved O&M strategies that take advantage of a range of innovations from robotic cleaning to “big data” analysis of performance data to identify issues and preventative interventions ahead of failures driving down O&M costs and reducing downtime. For the period 2018-2019, O&M cost estimates for utility-scale plants in the USA have been reported at between \$(10-18)/kW per year [8]. Recent costs there seem to be dominated by preventive maintenance and module cleaning, with these making up as much as 75% and 90% of the total, depending on the system type and configuration. The rest of the O&M costs can be attributed to unscheduled maintenance, land lease costs and other component replacement costs. The current benchmarks without inverter replacement are \$11.5/kW/year (residential), \$12.0/kW/year (commercial), \$9.1/kW/year (utility-scale, fixed-tilt), and \$10.4/ kW/year (utility-scale, tracking), significantly below previous O&M, only benchmark estimates [13]. Average utility-scale O&M costs in Europe have been recently reported at \$10/kW/year, with historical data for Germany suggesting O&M costs came down 85% between 2005 and 2017, to \$9/kW/year.

10. Results and discussion

PVWP configuration to supply water for irrigation to assist rural and remote areas in Albania was presented. This solution represents an alternative to simplify the installation process and to facilitate the PVWP, reducing the cost of electrical wiring network infrastructure design, installation time and maintenance. The

perspective of a wide use of green power motivates the scientific community to study the possibility of fabricating PV modules providing autonomous water pump systems for irrigation (PVWP).

11. Conclusion

The present paper highlights some aspects related to autonomous PVWP systems district, including an universal understanding of the actual irrigation used for crop cultivation in Divjaka region.

The existing diesel-powered water pumps and electricity from the national distribution line can be stand-by source option and should be replaced and combined in perfect harmony with PVWP extracting the maximum solar radiation.

The high costs of the actual systems coming from the distance from national electricity distribution lines have and fuel prices are the main problems that should be considered.

Being aware of the high share (73%) fossil fuel used in agriculture sector the only way to decarbonize the sector is using more RES technologies such as PV and wind sources.

From economic point of view off-grid PV systems for irrigation can be more effective and can bring low specific costs.

As a conclusion, off-grid PVWP concept should be the only option and solution in the way to deep decarbonisation of the agriculture sector in Albania and also promoting crop cultivation in the region.

References

- [1] Malka, L., Gjeta, A., Konomi, I., Alcani, M., Bebi, E., & Kaci, S. (2020). Off-grid hybrid PV configuration's role to supply internet access points antenna in remote areas. Case study: " Ostren i Vogel
- [2] IEA, "World Energy Investment 2019 Edition." (2019) and Sawle Y 2017 Review of hybrid renewable energy systems with comparative analysis of off-grid hybrid system Renewable and Sustainable Energy Reviews 81(2) 2217-35. <http://dx.doi.org/10.1016/j.rser.2017.06.033>
- [3] Renewable, International, and Energy Agency. 2020. Renewable Energy and Jobs – Annual Review 2020.
- [4] Wild-scholten, Mariska De. 2013. "Life Cycle Assessment of Photovoltaics Energy Payback Time Mono." (October)
- [5] Malka, Lorenc et al. 2020. "An Approach to the Large-Scale Integration of Wind Energy In." 10(5): 327–43.
- [6] Renewable energy market update, IEA, Paris <https://www.iea.org/reports/renewable-energy-market-update>
- [7] Energy, Renewable, I N Nationally, and Determined Contributions. UNTAPPED POTENTIAL FOR CLIMATE ACTION RENEWABLE ENERGY IN NATIONALLY
- [8] Malka, Lorenc et al. 2020. "An Approach to the Large-Scale Integration of Wind Energy In." 10(5): 327–43
- [9] IEA (2020), Renewable Power, IEA, Paris <https://www.iea.org/reports/renewable-power>
- [8] IEA (2020), Renewable Power, IEA, Paris <https://www.iea.org/reports/renewable-power>.
- [10] Jäger-Waldau, A., PV Status Report 2019, EUR 29938 EN, Publications Office of the European Union, Luxembourg, 2019, ISBN 978-92-76-12608-9, doi:10.2760/326629, JRC118058.
- [11] Renewable, International, and Energy Agency. 2019. RENEWABLE POWER GENERATION COSTS IN 2019
- [12] Leng, G., Dignard-Bailey, L., Bragagnolo, J., Tamizhmani, G. and Usher, E., Overview of the Worldwide Photovoltaic Industry, Report no. 96- 41- A1 (TR), CANMET Energy Diversification Research Laboratory, Natural Resources Canada, Varennes, QC, Canada, June 1996
- [13] Fu, Ran et al. 2018. "U.S. Solar Photovoltaic System Cost Benchmark: Q1 2018 U.S. Solar Photovoltaic System Cost Benchmark: Q1 2018." (November)

Investigation of the movement of a tomato plant during the transition between transport devices

Ivan Morteve

Institute of Soil Science, Agrotechnology and Plant Protection, Sofia – 1331

ABSTRACT: Mechanized harvesting of tomatoes should be carried out with minimal damage. This is achieved by knowing the processes. The movement of a tomato plant in the period of transition between conveying devices has been studied. Dependencies determining the length of free movement and the rates of fall on the fruit separator are derived, which are essential for determining the kinematic regime and preventing damage to the fruit.

KEY WORDS: TOMATO MECHANICAL HARVESTING, TOMATO PLANT MOTION, PARAMETER OF TOMATO PLANT MOTION.

INTRODUCTION

Tomatoes are a major vegetable crop subject to many research [Arazuri 2007, Zhang 2018, Mitova, 2018, Dimitrov, 2021]. In the case of mechanized harvesting of tomatoes, the plants are pruned from the soil surface and then go through various manipulations [Morteve, 2005]. All these manipulations must be performed with minimal losses and this is obtained with the correct choice of kinematic mode of the working devices. It is very common for them to move from one conveyor to another. In this regard, the aim of the present study is to determine the parameters of movement of a tomato plant during the transition period between the feed conveyor and the fruit separator, during mechanized harvesting.

ESSENCE OF THE STUDY

Previous studies [Morteve, 2008] have shown:

speed change laws

$$\dot{x}_{\Pi} = V_H \cos \alpha;$$

$$\dot{y}_{\Pi} = -gt + V_H \sin \alpha. \quad 1$$

speed change laws

$$x_{\Pi} = (V_H \cos \alpha)t;$$

$$y_{\Pi} = -g \frac{t^2}{2} + (V_H \sin \alpha)t + H_3. \quad 2$$

and the equation of motion of the tomato plant

$$y = -g \frac{x^2}{2V_H^2 \cos^2 \alpha} + xt \tan \alpha + H_3 \quad 3$$

Where g is the earth's acceleration;

α – angle of inclination of the conveyor to the horizontal plane;

H_3 – the height from the upper surface of the feed conveyor to the upper surface of the receiving conveyor;

V_H – initial speed at which the mass leaves the inclined conveyor and passes to the fruit separator. It is in fact the absolute speed of mass when it is on an inclined conveyor.

Equation (3) is the equation of the parabola. Through it some geometric and kinematic researches can be made. In this case, the length of the flight to the fruit separator is sought. For this purpose, the designations are entered (Fig. 1):

L is the maximum flight length provided that the plant does not meet the fruit-separating chains and continues its movement to the axis of the absolute coordinate system

L_H – the actual flight length of the plant from the feed conveyor to the fruit separator, measured from the point of intersection of the vertical plane at the point of separation of the plant from the feed conveyor and the plane of the fruit separator, to the point of falling of the plant on the fruit separator. In other words, this is the initial position in which the plant falls to be treated.

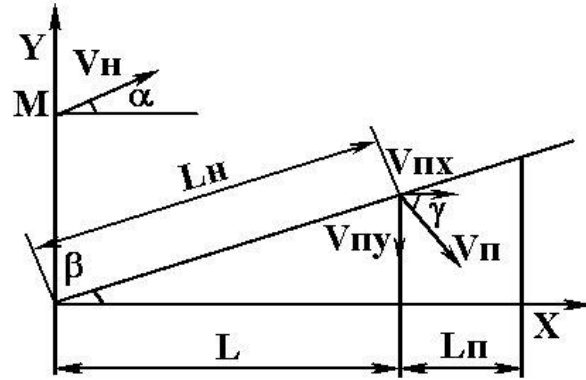


Fig.1. Indications of the flight parameters and the tomato plant from the inclined conveyor to the fruit separator.

The position in which the plant is on the axis of the coordinate system is sought. From this one can mathematically set the conditions:

$$y = 0; \quad x = L. \quad 4$$

Substituting conditions (4) in equation (3) gives:

$$-g \frac{L^2}{2V_H^2 \cos^2 \alpha} + Lt \tan \alpha + H_3 = 0 \quad 5$$

Equation (5) is quadratic [Danchev S., Rashkova I., 1994.] therefore has two roots:

$$L_{1,2} = \frac{-tg\alpha \pm \sqrt{tg^2\alpha - 4(-g/2V_H^2 \cos^2 \alpha)H_3}}{2(-g/2V_H^2 \cos^2 \alpha)}. \quad 6$$

After conversion:

$$L_{1,2} = \frac{-tg\alpha \pm \sqrt{tg^2\alpha + 2gH_3/V_H^2 \cos^2 \alpha}}{g/V_H^2 \cos^2 \alpha} \quad 7$$

From equation (7) it is clear that the second root is negative, which makes no practical sense. The positive root of the equation remains:

$$L = \frac{-tg\alpha + \sqrt{tg^2\alpha + 2gH_3/V_H^2 \cos^2 \alpha}}{g/V_H^2 \cos^2 \alpha} \quad 8$$

This is only the imaginary length of the flight that the plant would perform, provided that the fruit separator is not in motion and is not inclined at any angle to the horizontal plane (Fig. 1).

To reflect the adjustments, additional notations are introduced:

$t_{\Pi Y}$ is the conditional time during which the tomato plant is in flight from the feed conveyor to the axis X of the absolute coordinate system;

$t_{\Pi P}$ – the actual time during which the tomato plant is in flight from the feed conveyor to the plane of the fruit separator;

L_{Π} – the distance traveled by the separator and the entire machinery during the flight;

L_Y – the conditional path traveled by the plant over time $t_{\Pi Y}$.

When the plant is in a state of weightlessness or in other words in the air, the fruit-separating conveyor together with the whole machine moves gradually and follows a path determined by the formula:

$$L_{II} = V_M t_{IIY}. \quad 9$$

The conditional flight time can be determined by the end conditions in the selected coordinate system:

$$x = L; \quad y = 0. \quad 10$$

Substitute the conditions (10) in the system (2) and obtain:

$$L = (V_H \cos \alpha) t_{IIY};$$

$$-g \frac{t_{IIY}^2}{2} + (V_H \sin \alpha) t_{IIY} + H_3 = 0. \quad 11$$

It is easier to determine t_{IIY} by the first equation:

$$t_{IIY} = \frac{L}{V_H \cos \alpha} \quad 12$$

After placing (12) in (11) the distance traveled by the machine is determined:

$$L_{II} = \frac{V_M L}{V_H \cos \alpha} \quad 13$$

The total value of the coordinate x will be equal to the conditional path:

$$L_Y = L + L_{II} \quad 14$$

$$L_H = \frac{-tg\alpha + \sqrt{tg^2\alpha + 2gH_3/V_H^2 \cos^2\alpha}}{g \cos \beta / V_H^2 \cos^2\alpha} \left(1 + \frac{V_M}{V_H \cos \alpha}\right) \quad 19$$

After conversion, formula (19) takes the form:

$$L_H = \frac{-V_H \sin \alpha + \sqrt{V_H^2 \sin^2 \alpha + 2gH_3}}{g \cos \beta} (V_H \cos \alpha + V_M) \quad 20$$

The flight length determined by formula (20) provides information on the location of two adjacent conveyors.

Determination of the parameters of movement of tomato plants at the time of falling on the fruit-separating conveyor.

Once the dependencies related to the condition of the tomato plants have been determined before they are processed on the fruit separator, the main operation should be essentially moved on. It could not be said that this moment of fall is the beginning of the detachment of the fruit from the stems due to the fact that even in the field some varieties with a weaker connection between the fruit and the fruit bearing begin to crumble. This depends not only on the variety, but also on many other features related to agricultural techniques and cultivation technology. In addition, fruits can be torn off when the plants are pruned, picked up by the inclined conveyor, and also by the action of other elements of the tomato harvester. But basically the process of fruit separation takes place on the designated node. For this reason, fruiting is considered from the moment the plant falls on it. Dependencies for determining the rates of fall have been derived to be taken into account when determining the kinematic regime of the fruit separator. The aim is to link the kinematic regime with some of the physical and mechanical properties of tomato plants and fruits in order to avoid damage and loss of production.

Determining the rate of fall of the plant on the surface of the fruit separator.

When the plant falls into the plant mass, impulses appear, which are able to tear off some fruits. To determine this speed, the notations are entered:

V_{XII} is the projection along the axis x of the speed of the plant at the time of falling on the fruit separator.

V_{YII} — the projection along the axis y of the speed of the plant at the time of falling on the fruit separator.

Substitute equation (13) in (14) and obtain:

$$L_Y = L + \frac{V_M L}{V_H \cos \alpha}. \quad 15$$

After conversion of (15) by exporting L outside the brackets is obtained (16)

$$L_Y = L \left(1 + \frac{V_M}{V_H \cos \alpha}\right) \quad 16$$

From the conditional length of the flight it is necessary to determine the actual. Once the precondition for the movement of the fruit-separating plane has been taken into account, it is necessary to take into account the angle of inclination of the same plane. For this purpose, a trigonometric function will be used (Fig. 1), from which it follows:

$$L_H = \frac{L_Y}{\cos \beta} \quad 17$$

Substitute equation (16) in (17) and obtain:

$$L_H = \frac{L}{\cos \beta} \left(1 + \frac{V_M}{V_H \cos \alpha}\right) \quad 18$$

Substitute equation (8) in (18) and obtain the final expression (19) for the length of the fruit separator, which is not used for its intended purpose, as the plant is in flight above it before it is located on the fruit-dividing plane for cultivation.

γ — the angle of absolute velocity of the plant at the time of its fall on the fruit separator relative to the horizontal plane.

It is based on the laws of variation of speed, from the system (1):

From here the horizontal component of the speed is known, but to find the vertical component it takes time to fly t_{IIP} . To determine it is based on the final conditions:

$$x = L_H \cos \beta; \quad y = L_H \sin \beta. \quad 21$$

Substitute the conditions (21) in the law of motion system (2) and obtain:

$$L_H \cos \beta = (V_H \cos \alpha) t_{IIP};$$

$$t_{IIP} = -g \frac{t_{IIP}^2}{2} + (V_H \sin \alpha) t_{IIP} + H_3. \quad 22$$

It would be easier to find t_{IIP} from the first equation:

$$t_{IIP} = \frac{L_H \cos \beta}{V_H \cos \alpha} \quad 23$$

Substitute (23) in (1) the components of the velocities at the moment of fall are obtained:

$$V_{XII} = V_H \cos \alpha;$$

$$V_{YII} = -g \frac{L_H \cos \beta}{V_H \cos \alpha} + V_H \sin \alpha. \quad 24$$

From the components thus obtained, the absolute speed of fall can be found V_{AII} :

$$V_{AII} = \sqrt{V_{XII}^2 + V_{YII}^2} = \sqrt{V_H^2 \cos^2 \alpha + \left(-g \frac{L_H \cos \beta}{V_H \cos \alpha} + V_H \sin \alpha \right)^2} \quad 25$$

The absolute speed of fall is an important characteristic that determines the strength of the impact of the elements of the conveyor on the fruit and from there determines the damage to the fruit and the quality of production.

$$\gamma = \arctg \frac{V_{YII}}{V_{XII}} = \arctg \frac{-g \frac{L_H \cos \beta}{V_H \cos \alpha} + V_H \sin \alpha}{V_H \cos \alpha} \quad 26$$

After bringing under a common denominator and reductions in the trigonometric function is obtained for the angle between the absolute velocity of the plant at the time of its fall on the fruit separator with the horizontal plane (27)

$$\gamma = \arctg \left(-g L_H \cos \beta + V_H^2 \sin \alpha \cos \alpha \right) \quad 27$$

The derived dependences make it possible to establish the characteristics of the movement of tomato plants at the time of submission for fruit separation. The characteristics of the movement can be used to determine the kinematic regimes of the mechanisms in which the damage will be minimized.

CONCLUSIONS

1. In the transition between the feed conveyor and the fruit separator, the tomato plants are in free movement with a flight length determined by formula 20. This provides information on how to place two adjacent conveyors and determine the technological lengths of the conveyors.
2. The absolute speed of fall of the fruit formula 25 is an important characteristic that determines the strength of the impact of the elements of the conveyor on the fruit and from there determines the damage to the fruit and the quality of production.
3. The derived dependencies make it possible to establish the characteristics of the movement of tomato plants at the time of submission for fruit separation.
4. The characteristics of the movement may be used to determine the kinematic regimes of the mechanisms in which damage to the fruit will not occur or will be minimized.

LITERATURE

1. Dimitrov., Em., Petrova, V., 2021. Influence of the irrigation regime on the yield of determinant tomato variety

The angle γ between the speed of fall V_{AII} and the positive direction of the abscissa is determined by a trigonometric function:

"Nikolina" F1 in Polish production. Proceedings "Ecology and Agrotechnology - Basic Science and Practical Implementation", pp.160-166, ISSN 2683-0663.Bg

2. Mitova, I., Vessela Petrova - Branicheva, Emil Dimitrov, Influence of fertigation on some factors determining the quality of tomatoes variety "Nikolina F1", Soil agrochemistry and ecology, 52, 3/2018 Bg

3. Danchev S., Rashkova I., Handbook of Elementary Mathematics, Sofia 1994. Bg

4. Morteve, IE, Mechanized harvesting of tomatoes, scientific journal of agricultural and forestry science, issue. 2-3, 2005, p114. Bg

5. Morteve, Iv. E., Movement of a tomato plant before submission for fruit separation in a tomato harvester, Agricultural machinery, no. 1, 2008. ISSN: 0037-1718, Sofia, pp. 9-13. Bg

6. Pisarev, A., Mechanical vibrations, Sofia 1985. Bg

7. Pisarev, AM, Paraskov CN, Bachvarov SN, Course in Theoretical Mechanics Part II Dynamics, Sofia 1975. Bg

8. Arazuri, S., C.Jarén, J.I.Arana,J.J.Pérez de Ciriza, Influence of mechanical harvest on the physical properties of processing tomato (*Lycopersicon esculentum* Mill.) Journal of Food Engineering, Volume 80, Issue 1, May 2007, Pages 190-198

9. Karakolev et al., Tomato picking machine, United States Patent No 4,727,714 Int. Cl. A01D 45/00.

10. Zhang, Baohua, JunZhou, YimengMeng, NaZhang, BaoxingGu, Zhenghong, YanSunusi, IdrisIdris, Comparative study of mechanical damage caused by a two-finger tomato gripper with different robotic grasping patterns for harvesting robots, Biosystems Engineering, Volume 171, July 2018, Pages 245-257

Studies to establish the evapotranspiration of strawberries grown in open areas

Rumiana Kireva, Miho Mihov

Institute of Soil Science, AgroTechnology and Plant Protection "Nikola Pushkarov", Sofia, Bulgaria

Email: R.Kireva@abv.bg ; M.Mihov@abv.bg

Summary Evapotranspiration of strawberry, remontant variety "Polka" (field production) was established in a three-year field experiment (2011-2013) drip irrigation on leached cinnamon forest soil in the area of the village of Chelopechene, Sofia region. Various irrigation regimes have been tested - from full satisfaction of the daily needs of the crop from water to irrigation with reduced by 20% and 40% irrigation rates.

On average for the research period the size of the total evapotranspiration for the vegetation period of strawberry is 240 mm, as its main part is formed by the irrigation norm - 58%, and the rest of the precipitation - 42%. The average daily values vary by ten days, with the highest values reaching the first and second ten days of June (harvest period). Values of the biophysical coefficient Z necessary for determining the design irrigation regime and forecasting the time for irrigation of the crop have been determined.

Introduction

Evapotranspiration (ET) of any agricultural crop (including that of strawberries) is a major cost element in the water balance of the active soil layer and is one of the main factors determining the parameters of the irrigation regime. The intensity of ET directly affects the duration of the irrigation period, and hence the number of irrigations and the size of the irrigation rate.

For the conditions of our country the total evapotranspiration (ET) of strawberries during the growing season is 750 -810mm for areas with lower altitude, while for the foothills it is 10-15% lower, as the requirements of plants during the growing season to water are different. They are the most demanding in fruit ripening and ripening (2). The results of research conducted in the conditions of our country prove that it is reasonable and correct to calculate evapotranspiration by a formula based on the sum of the average daily air temperature. (2.4)

The aim of the study is to determine the amount of evapotranspiration of strawberries grown under drip irrigation on cinnamon forest soil (leached) in Sofia field.

Research methodology

To establish the evapotranspiration of strawberries variety "Polka" in the period 2011-2013, a field experiment was conducted on an experimental field of ISSAPP "N. Pushkarov" Chelopechene, Sofia

The following variants of irrigation at pre-flood humidity were tested - 85% of Field Capacity:

1. 100% realization of the irrigation rate;
2. 80% realization of the irrigation rate;
3. 60% realization of the irrigation rate.

The experimental determination of the evapotranspiration of strawberries for the growing season was made on the basis of data on the dynamics of soil moisture during the growing season and irrigation for option 1 for soil layer 0-50 cm depth at which layer is more than 85% of the main root system of strawberries, by the method of water balance was established evapotranspiration of strawberries for the first "productive" growing season, ie. , April - June.

The water balance calculations were performed according to the formula:

$$ET = W_{нач} - W_{кп} + m , \quad (1)$$

where: ET is evapotranspiration, mm;

$W_{нач}$ – the water reserve in the layer 0-50 cm at the beginning of the period for which the ET is calculated, mm;

$W_{кп}$ – the water supply in the layer 0-50 cm at the end of the period in mm;

m – irrigation rate in mm / m².

From the data for the evapotranspiration of the culture (strawberries) the daily values of the biophysical coefficient Z (1) are calculated according to the following formula:

$$ET = Z \cdot \sum t, \quad Z = \frac{ET}{\sum t} \quad (2)$$

where ET is evapotranspiration, mm;

$\sum t$ – the ten-day sum of the average daily air temperatures in °C;

Z – the biophysical coefficient, which is determined for each crop separately depending on the final temperature sum of the period.

Results and discussions

Evapotranspiration of the crop varies by year and depends on weather conditions. It reached its highest values in 2013 - 265 mm, and in the other two years the values are close to 192 mm for 2011 and 247 mm for 2012. This is due to the close meteorological conditions of the years (Table 1). On average for the research period the size of the total ET for the vegetation period of strawberries is 240 mm (Table 1).

In order to properly meet the needs of plants for water, it is necessary to establish the course of the dynamics of evapotranspiration by ten days and the average for the study period.

Practical value related to the forecast has the option with the submitted optimal irrigation rate. June, (Fig. 1).

On average for the experimental years, the average daily values of evapotranspiration vary from 1.6 to 4.8 mm, and in the initial phase of the development of the culture values are lower due to the smaller size of plants that consume insignificant amounts of water and the lower evaporative capacity of the atmosphere.

When optimizing the soil moisture, the water consumption of the strawberry increases, as the degree of increase depends on the climatic situation during the experimental year and the number of realized irrigations. With the entry of strawberries in the phase of intensive growth, which begins in May, there is a more intense increase in ET, and by the second and third decade of May it reaches 3.5 - 4.5 mm on average for the study period. The maximum daily averages of evapotranspiration are associated with the period of ripening, fruit picking, which coincides with a period of high evaporation capacity of the atmosphere. This period covers June. The maximum of ET is in the first ten days of June. In the individual years it varies from 4.5 to 4.8 mm (Table 1 and Fig. 2).

The changes in the average daily values of evapotranspiration during the growing period follow the development of the culture and the changes of the meteorological factors.

The calculated daily values of the biophysical coefficient Z based on experimental determination of evapotranspiration and the daily sums of the average daily air temperature calculated by the formula of [2] are presented in (Table 1 and Fig. 3). Changes in the values of this coefficient follow the changes in evapotranspiration during the growing season of the crop and reflect the specifics of water consumption depending on the biological requirements of the crop, phase of development, manifestations of meteorological factors. of the project irrigation regime and forecasting the time for irrigation of the crop.

On the average for the experimental period, the values of the biophysical coefficient Z of the crop vary from 0.14 to 0.29, being

the lowest at the beginning of the vegetation and the highest during the formation and ripening of the fruits. These results provide a real opportunity to develop the design and operational irrigation regime

of strawberry plantations in conditions of water deficit, using the bioclimatic method.

Table 1 Evapotranspiration of strawberries during the growing season

Months	ten day periods	/Evapotranspiration, mm/day				biological coef
		2011	2012	2013	Average for the period	average for the period
		Average daily mm/day	Average daily mm/day	Average daily mm/day	Average daily mm/day	ten days periods
April	2	1,5	1,8	1,5	1,6	0,14
	3	1,7	2,1	2,0	1,9	0,16
May	1	2,3	2,8	3,1	2,7	0,18
	2	2,8	3,5	4,2	3,5	0,23
	3	3,4	4,2	5,5	4,5	0,29
June	1	4,1	4,8	5,5	4,8	0,25
	2	4,6	5,1	4,2	4,6	0,23
ET total for growing season		192	246	265	240	average 0,21

ET средноденонощна / Evapotranspiration. mm/day

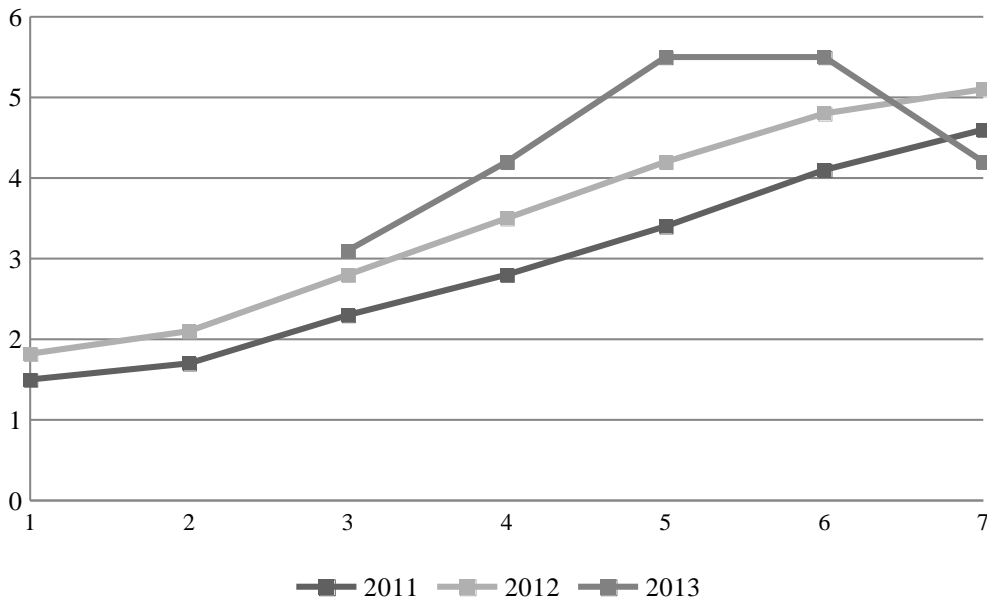


Fig. 1. Average daily evapotranspiration by years

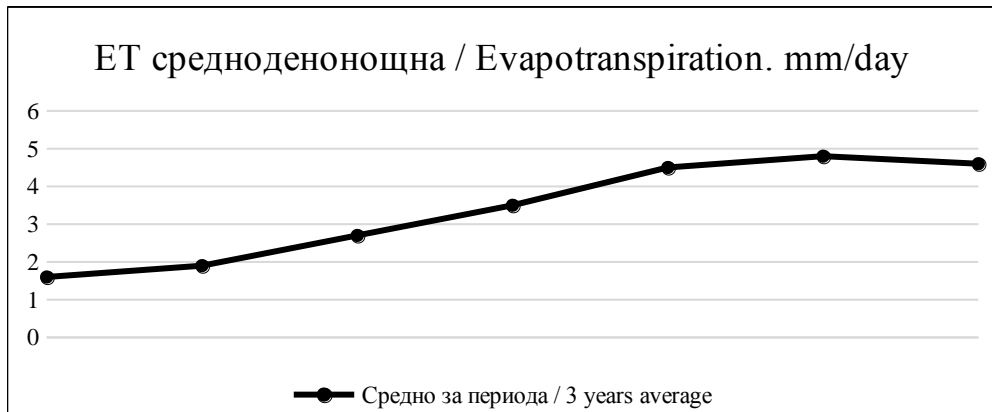


Figure 2. Average daily evapotranspiration average for 2011-2013

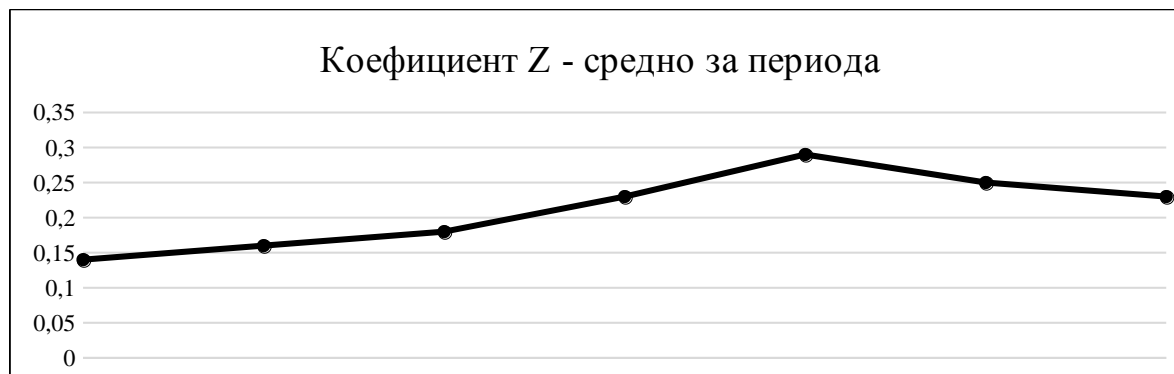


Fig.3 Values of the biophysical coefficient Z on average for the period 2011-2013

Table 2 Total evapotranspiration and forming elements of strawberries (field production) (2011-2013)

years	Total evapotranspiration, mm	forming elements of evapotranspiration	
		irrigation rate, % of ET	rainfall % of ET
2011	192	79	21
2012	246	49	51
2013	265	54	46
Average(2011-2013)	240	58	42

The percentage of the forming elements of ET varies from year to year and depends on meteorological factors. The largest share in the formation of ET is occupied by the irrigation norm in 2011 (dry), as its percentage share reaches 79%, and in the remaining 21%, precipitation participates. (Table 2)

Conclusions

On average for the research period, the size of the total evapotranspiration for the vegetation period of strawberries is 240 mm, as the main part is formed by the irrigation norm - 58%, and the rest of the precipitation - 42%.

The established average daily values of evapotranspiration in the individual years vary from 1.5 to 5.5 mm and reach maximum values in the first ten days of June (ripening period, fruit picking).

The course of the changes of the average daily values of evapotranspiration during the vegetation period follows the development of the culture and the changes of the meteorological factors.

The determined values of the biophysical coefficient Z represent an objective basis for determining the design irrigation regime and forecasting the time for irrigation of the crop.

References

1. Y., H.Hristov, Iv.Zonev, 1962. Design irrigation scheduling for agricultural crops. Ppoc.-IHM,3, p.5-56, (Bg).
2. Zahariev, T., 1985. On Methods and Formulas for Determining the Evapotranspiration of Agricultural Cultures, in Support of Technical Progress in Water Management, vol. 2, p.3-10, (Bg).
3. Ivanov, Al., 1998. Studies on irrigation of strawberry, raspberry and blackcurrant by dropping, Habilitation work, Kostinbrod, p.51, (Bg).
4. Sp., 1991. Participates in the groundwater in the eutonpression of agricultural crops., Dissertation, p.134, (Bg).